INTERNATIONAL JOURNAL OF AUTOMOTIVE AND MECHANICAL ENGINEERING
ISSN: 2229-8649 e-ISSN: 2180-1606
VOL. 20, ISSUE 2, 2023, 10574 – 10594
DOI: https://doi.org/10.15282/ ijame.20.3.2023.02.0816

اونيۏرسيتي مليسيا ڤهڠ
UNIVERSITI MALAYSIA PAHANG

RESEARCH ARTICLE

Dynamic Testing of In-Wheel Motor Based Electric Vehicle in Longitudinal Direction

M. S. Azizi Razak[1], F. Ahmad[1,*], M. H. Che Hasan[2] and H. Jamaluddin[3]

[1]Faculty of Mechanical Engineering, Universiti Teknikal Malaysia Melaka, 75450 Melaka, Malaysia
[2]Faculty of Electrical and Electronics Engineering Technology, Universiti Teknikal Malaysia Melaka, 75450 Melaka, Malaysia
[3]Faculty of Engineering and Information Technology, Southern University College, 81300 Johor, Malaysia

ABSTRACT - This paper presents an investigation into the performance of in-wheel motor (IWM) based electric vehicles (IWM-EV) in the longitudinal direction. The design of IWM-EV is an innovation of the conventional go-kart vehicle with slight modifications in steering, suspension, and braking system, which then makes use of a three-phase permanent magnet synchronous in-wheel motor (PMSM-IWM) at both of the rear axle wheels. An extension of that is a simulation of an IWM-EV vehicle using a 5-degree-of-freedom vehicle longitudinal model that has been developed by incorporating PMSM-IWM as a drive wheel located at the rear axles. Using the simulation, vehicle dynamic control in the longitudinal direction-based Proportional-Integral-Derivative (PID) controller has also been strategized. With the intention to confirm the capability of the IWM-EV, experimental studies-based real IWM-EV hardware have been conducted. Three dynamic tests that generalized from SAE standard SAE J866-199908, namely acceleration performance at the level pavement (including acceleration tests and acceleration then braking tests) and road gradient tests at constant speeds of 10, 15 and 20 km/h, were used as the testing method. The performance areas evaluated were vehicle body speed, wheel speed, distance travel experienced by the vehicle, IWMs current, drive torque, as the battery voltage capacity used by the vehicle. The findings indicate that the simulation results and experimental data are similar, with less than 5 % error. The outcomes from this study can be considered in the design optimization of a torque vectoring control in the next research study.

ARTICLE HISTORY
Received : 14th March 2023
Revised : 07th July 2023
Accepted : 02nd Aug 2023
Published : 26th Sept 2023

KEYWORDS
Individual PMSM motor;
In-wheel motor;
Electric vehicle;
Longitudinal control;
Experimental testing

1.0 INTRODUCTION

The motivation for this study lies in the increasing requisition for minimal environmental impact vehicles with adequate performance traits. Although still effective in their use, internal combustion engine (ICE) vehicles have become the main contributors to greenhouse gas emissions, air pollution, carbon monoxide, and air toxins [1-3]. With a significantly less profound impact on the environment than ICE vehicles, electric vehicles are considered a technology that could meet the demand for low environmental impact vehicles [2-4]. Thus, the development of electric ground vehicles (EVs) has emerged as a burgeoning area of research in both academia and commercial research. This has resulted in noteworthy enhancements in the handling of passenger vehicles, energy usage, and control technology has been achieved. Moreover, EVs also support the vision of x-by-wire, where a multipoint bus network emancipates vehicle control from the constraints of mechanical linkages. This approach can also enhance cabin space with ergonomic and crash-compatible controls [5]. Looking further ahead, this system has the potential to support autonomous vehicles [6-7].

Compared to ICE-based vehicles, EVs may use different configurations, which can have a profound impact on the vehicle's performance and efficiency characteristics. One configuration of EVs that has demonstrated perfect outcomes in vehicle performance traits is utilizing independently actuated in-wheel motors (IWM) [8-10]. These IWMs allow for the enhancement of vehicle control, as they are part of the vehicle's unsprung mass and can be utilized to actively design performance features instead of tuning them indirectly through the conventional chassis system.[7]. The utilization of IWMs allows for better accuracy in measuring vehicle characteristics, as each IWM has its sensor to measure independent wheel speed resulting from accurate and fast torque generation. Indirectly, it indicates that the vehicle's dynamic behavior and road surface conditions can be more precisely measured and estimated, enabling the vehicle to optimize its torque allocation and enhance its performance.

To date, although some successes have been recorded, in-wheel motor-based electric vehicle technology (IWM-EV) is a relatively young, emerging, but advanced technology with very broad expansion prospects. However, there are still some shortcomings in the use of IWM on real vehicles, which then the investigation into this topic. According to preliminary analysis, some of the weaknesses and shortcomings of this technology are as follows: in recent years, several subsequent studies on IWM-EV systems have been rapidly developed for different purposes and requirements [11-12], [13-19]. Although the results have contributed significantly to the development of knowledge about IWM-EV, the results

*CORRESPONDING AUTHOR | F. Ahmad| ✉ fauzi.ahmad@utem.edu.my

are still weak and questionable. This is because the tests conducted on IWM-EV capabilities are still limited to simulation-based tests [6], [8], [20] and HILS methods [14], [21-23] that require some simplification, justification, and assumptions during the tests. It is common knowledge that justification and assumptions may inaccurately reflect the data and likely result in inaccurate predictions [24]. This is also confirmed by other researchers [25-28], who state that a situation's measurement through simulation is useless until it is confirmed with experimental tests through real systems.

If it is investigated in-depth, this can be considered to be caused by the control system that has used advanced control strategy such as Fuzzy Logic Control (FLC) based torque and speed controller [29-32], Neural Network (NN) based electronic differential control strategy [29], [31], [33–34], genetic algorithm [35-38], sliding mode control (SMC) [39–48] Although it can be said to be successful in the simulation system, it is widely acknowledged that those proposed controllers have some limitations, such as static rules in FLC [24-25], complex iteration in NN [33-34], [38], and slow learning speed in SMC [44-48] which are difficult to be implemented in a microcontroller and difficult to realize, thus causes the potential benefits of IWM-EV cannot be fully exploited. However, only a limited number of experimental studies yielded positive outcomes, but they were subject to significant constraints where the experimental results obtained did not align with the theoretical predictions and exhibited response delays due to system damage and security issues. [49-50]. The successful experimental studies of IWM-EV are mostly made by vehicle manufacturing companies: Nissan Motor Corporation, ELAPHE LTD, Aptera Motors Corp, Protean Electric, and EV Central. At the same time, academic organizations recorded very few successful studies because of system malfunction in case of failure problems and safety issues due to the absence of a suitable test site.

To contribute to the development of EVs in particular, an IWM-EV has been developed in the Autotronic Laboratory Faculty of Mechanical Engineering UTeM. Basically, the design of the IWM-EV is an innovation of the conventional go-kart vehicle with slight modifications in steering, suspension, and braking system. Besides, the power terrain of the vehicle has been changed by integrating IWMs at the rear axle wheels. To that end, IWM-EV-based simulation and longitudinal dynamic control were developed using MATLAB Simulink Software. With the intention to confirm the capability of the IWM-EV, experimental studies-based SAE standards have been conducted, gathered, and compared with the simulation results. This paper is organized into five sections as follows: the first section includes an introduction, a scrutiny of pertinent preliminary work, and an assessment of the IWM-EV's performance. Section two introduces the mathematical equations that are used to develop the simulation model, hardware, necessary instrumentation, and data acquisition system for experimental study, followed by the basic erudition on the determination of vehicle center of gravity. The third section delved into the control strategy and the simulation parameters imposed on the IWM-EV. The fourth section presents the results obtained using simulation and experimental study, and finally, the study's conclusion is presented in the last section.

2.0 MATHEMATICAL MODEL OF THE IN-WHEEL MOTOR-BASED ELECTRIC VEHICLE

The development of the IWM-based electric vehicle is started via a simulation method based on the 5 degrees of freedom (5-DOF) vehicle model illustrated in Figure 1. With the assumption that the vehicle consists of a sprung mass connected to four unsprung masses through the suspension system, the vehicle is only subjected to a longitudinal dynamic [26], [51]. Note that the suspension system is modelled as a rigid body that prevents the unsprung mass from bouncing vertically, thus precluding the sprung mass's ability to pitch, roll and bounce. Besides, the vehicle is assumed to be a front wheels steer [52], where each of the unsprung masses is permitted to rotate on its axis, and only two IWMs are used at the rear axle of the wheels.

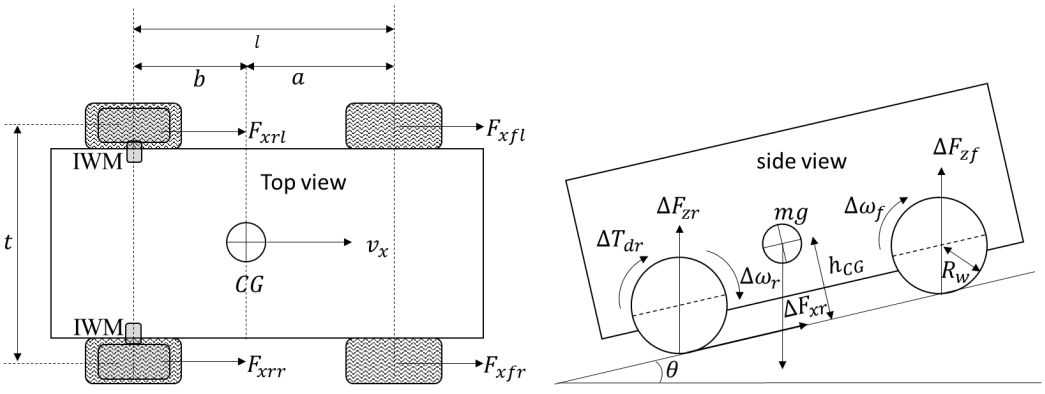

Figure 1. 5 DOF vehicle model

As shown in Figure 1, the dynamic of the vehicle is given by:

$$\boldsymbol{m\dot{v}_x = \sum F_x + mg\sin\theta + F_d} \tag{1}$$

where, m is the vehicle mass, g is the gravitational acceleration, θ is the road gradient, $\sum F_x$ is the summation of longitudinal force acting on the rear left and right tires that is denoted as F_{xrl} and F_{xrr} respectively. F_d is the drag force and is represented by

$$F_d = \frac{1}{2}\rho {v_x}^2 C_D A \tag{2}$$

where A is defined as the frontal area, ρ is calculated from the density of air, v_x is the longitudinal velocity and C_D is the aerodynamic drag coefficient. During dynamic, there are reaction forces under each of the front and rear tires, whereby the front tyres can be described as F_{zf}, and while the rear tires it is elucidated as F_{zr}.

$$F_{zf} = \frac{1}{2}mg\left[\frac{b}{l}\cos\theta + \frac{h_{cg}}{l}\sin\theta\right] - \frac{1}{2}m\dot{v}_x\frac{h}{l} \tag{3}$$

$$F_{zr} = \frac{1}{2}mg\left[\frac{a}{l}\cos\theta + \frac{h_{cg}}{l}\sin\theta\right] - \frac{1}{2}m\dot{v}_x\frac{h}{l} \tag{4}$$

Here, a is defined as the distance of the CG from the front axle, b is the distance of the CG from the rear axle, and l is the vehicle's wheelbase. Assumed that the IWM and braking system are applied at the rear wheels only, the dynamic motion of the wheels can be written as:

rear wheels,

$$\boldsymbol{J\dot{\omega}_r = \Delta T_{dr} - \Delta F_{xr} R_w - T_{br}} \tag{5}$$

and front wheels,

$$\boldsymbol{J\dot{\omega}_f = -\Delta F_{xf} R_w} \tag{6}$$

where, T_{br} is the rear wheel brake torque, R_w is the wheel radius and T_{dr} is the drive torque provided by the three-phase IWM, which can be expressed as:

$$\boldsymbol{T_{dr} = P[(L_d - L_q)i_d i_q + \psi_f i_q]} \tag{7}$$

that generalized from

$$\boldsymbol{V_d = R_s i_d + P\psi_d - \omega_r \psi_q} \tag{8}$$

$$\boldsymbol{V_q = R_s i_q + P\psi_q - \omega_r \psi_d} \tag{9}$$

$$\boldsymbol{\psi_d = L_d i_d + \psi_f} \tag{10}$$

$$\boldsymbol{\psi_q = L_q i_q} \tag{11}$$

here V_d and v_q are the stator voltage on the dq-axis, L_d and L_q are the synchronous inductances from the contribution of the two-phase currents, R_s is the stator resistance, ω_r is the rotor angular speed, P is the number of rotor poles pair, i_d, i_q and ψ_d, ψ_q is the stator current and stator flux on the dq-axis, respectively, as shown in Figure 2.

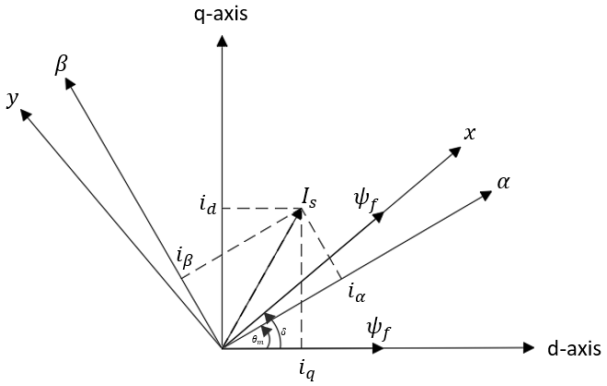

Figure 2. IWM vector diagram

while the flux linkage equation at dq-axis is derived from:

$$\psi_a = L_{aa}i_a + L_{ab}i_b + L_{ac}i_c + \psi_{ma} \tag{12}$$

$$\psi_b = L_{ab}i_a + L_{bb}i_b + L_{bc}i_c + \psi_{mb} \tag{13}$$

$$\psi_c = L_{ac} i_a + L_{bc} i_b + L_{cc} i_c + \psi_{mc} \tag{14}$$

where the v_a, v_b and v_c is the three-phase voltage; R_a, R_b and R_c is the resistance of coils A, B, and C, i_a, i_b and i_c is the three phase current; P is the number of pole; ψ_a, ψ_b and ψ_c is the flux of coils A, B, and C; L_{aa}, L_{bb} and L_{cc} is denoted as self-inductance; L_{ab}, L_{ac} and L_{bc} is considered as the symmetry of mutual inductance and ψ_{ma}, ψ_{mb} and ψ_{mc} represent the flux linkage on coils A, B, and C. The electrical dynamics equation [53] in terms of phase variable can be written as:

$$V_a = R_a i_a + P\psi_a \tag{15}$$

$$V_b = R_b i_b + P\psi_b \tag{16}$$

$$V_c = R_c i_c + P\psi_c \tag{17}$$

The model of the PMSM IWM was then simplified into a transfer function, which is developed based on the training data of voltage and wheel speed and is expressed as follows:

$$G(s) = \frac{34.79\, s + 1.844}{s^2 + 1.774\, s + 0.08779} \tag{18}$$

As the vehicle chassis is directly linked to the wheel, it can be presumed that the longitudinal speed of the wheel corresponds to that of the vehicle. However, once a vehicle's brakes are applied, it generates a braking force at the contact point between the wheels and the road surface [54-55], which leads to a decrease in the wheel's rotational velocity. Since the force (friction) acting on the wheel increases, the wheel will experience slippage against the road surface, resulting in the wheel speed being lower than the vehicle's speed. This condition is identified as the longitudinal tire slip (S), and mathematically, it can be described as equation follows:

$$s = \frac{v_x - \omega R_w}{\max\,(v_x, \omega R_w)} \tag{19}$$

Several empirical functions, known as B, C, D, and E, are used to describe the nonlinear relationship between longitudinal force and slip ratio, where B represents the stiffness factor, C denotes the form factor, D indicates the peak factor, and E refers to curvature factor, which Pacejka originally proposed [56]. This formula is given by:

$$f_x(S) = A \sin[B\ tan^{-1}(CS - D(CS - tan^{-1}(CS))] \tag{20}$$

The longitudinal force can be expressed by

$$f_x(S) = \begin{cases} f_x(s) & : S \geq 0 \\ -f_x(S): & S < 0 \end{cases} \tag{21}$$

In order to construct an accurate vehicle simulation model, a hydraulic brake model has been designed based on prior research works, namely Gerdes et al. [57] and Aparow et al. [58]. It can be found that the pressure exerted on the disc brake can be expressed as follows.

$$P_b = 1.5 K_c u_b - \tau_{bs} \dot{P}_b \tag{22}$$

where P_b is the applied brake pressure, K_c is the simple pressure gain, u_b is the brake setting and τ_{bs} is the brake lag. By considering ϑ is as the simple pressure gain and K_b is the cylinder pressure gain, the brake torque can be calculated as:

$$T_b = P_b K_b \min\left(1, \frac{\omega}{\vartheta}\right) \tag{23}$$

All of the equations for the IWM and vehicle model have been designed in the MATLAB/Simulink software and can be referred in Figure 16 and Figure 17 in Appendix D.

2.1 Hardware, Instrumentation, Parameter Acquisition and Experimental Setup

Figure 3 shows the IWM-based electric vehicle experimental hardware that has been developed in Autotronic Laboratory UTeM. A set of data acquisition systems (DAS) was installed on the vehicle to acquire genuine vehicle feedback during dynamic. It utilizes various types of transducers, such as an accelerometer and gyroscope sensor (MPU6050), which have a tri-axis accelerometer and gyroscope to measure longitudinal, vertical, and lateral accelerations as well as pitch rate, roll rate, and yaw rate at the body centre of gravity, an adjustable potentiometer 10 K Ω to sense the brake and throttle input, and current sensors (ACS712) with 20A maximum limit to sense the current providing by the IWMs. Besides that, four-wheel speed sensors have been used to sense the angular speed of the wheels, while PS-3 brake and throttle pedal were used to provide the throttle and brake input to the vehicle. A voltage sensor (B25) is also used to measure the battery voltage consumed by the IWM, while a hall sensor will measure the speed of the IWM. Noted that, in this experimental vehicle, Arduino Uno R3 type together with PWM to analogue converter has been used as the electronic control unit as well as the data logger. All of the aforementioned transducers employ a 5 V DC power supply and a current level below the threshold of 1.0 A. The data has been sent to the MATLAB software and logged by using a Simulink scheme, as depicted in Figure 18 and Figure 19 in Appendix D.

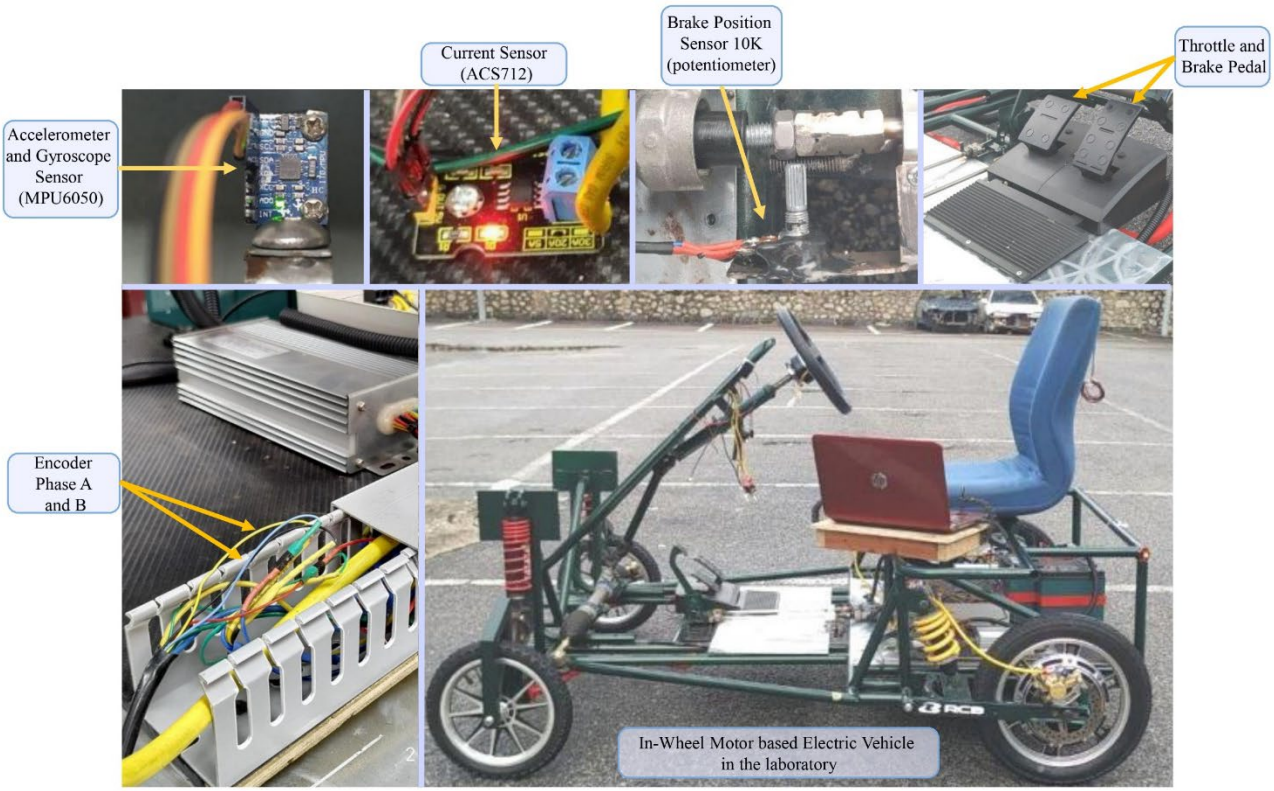

Figure 3. IWM-based electric vehicle

In extension to this process, a study was performed experimentally to assess the position of CG (centre of gravity). The parameters that were monitored include the position of CG from the front and rear axle as well as its height from the ground, which are marked as a, b and h_{cg} respectively, as shown in Figure 4(a). In order to determine the parameters a and b, the weight of the car and the force under each front and rear wheel have been measured using 12V FUTEK load cell LCF451(L2903) depicted in Figure 4(a).

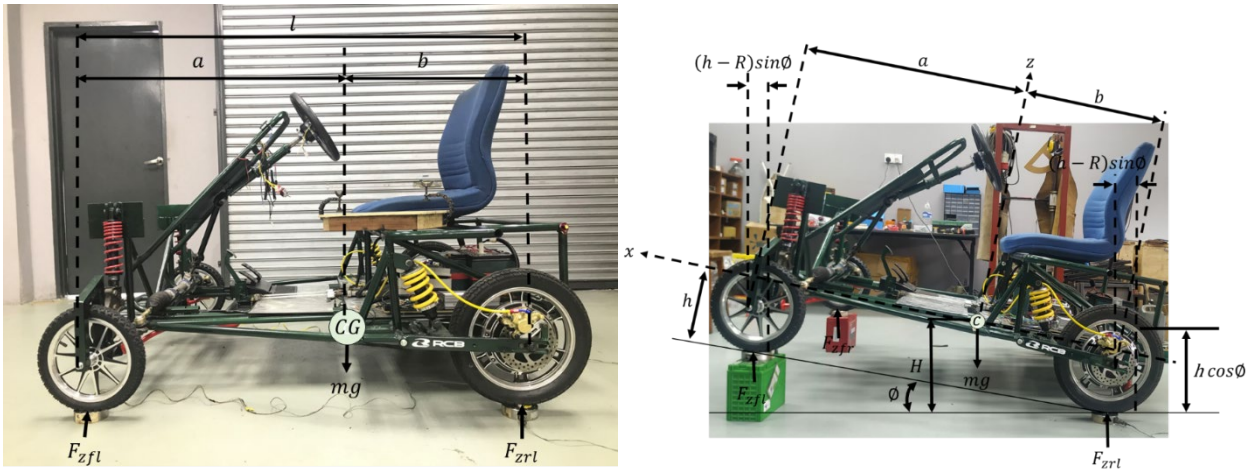

(a) (b)

Figure 4. Vehicle parked (a) on level pavement and (b) on an inclined surface

By assuming the force under the front wheels are ΔF_{zf} and rear wheels are ΔF_{zr}, the position of the CG is calculated by applying the static equilibrium equations defined by $\sum F_z = 0$ and $\sum M_{cg} = 0$, thus

$$\boldsymbol{a = \frac{l}{mg}\Delta F_{zr}} \tag{24}$$

and

$$\boldsymbol{b = \frac{l}{mg}\Delta F_{zf}} \tag{25}$$

while by scaling the vehicle on an inclined surface, shown in Figure 4(b), the h_{cg} can be described as:

$$h_{cg} = \frac{\Delta F_{zr}(l)}{mg} - a\cos\left(\sin^{-1}\frac{H}{l}\right) + \frac{R_f + R_r}{2} \tag{26}$$

where H is the height of the front axle, R_f and R_r are the radius of the front and rear wheels, respectively. Based on the examinations and observation, the parameters of the vehicle utilized in the simulation are listed in Table 1.

Table 1. IWM-electric vehicle parameter

Parameter	Symbol	Value
Vehicle		
Track width	t	1.25 m
Wheelbase,	l	1.35 m
Distance front axle to CG	a	0.82 m
Distance rear axle to CG	b	0.53 m
Normal force under front left tire	F_{zfl}	255.06 N
Normal force under front right tire	F_{zfr}	255.06 N
Normal force under rear left tire	F_{zrl}	392.40 N
Normal force under rear right tire	F_{zrr}	392.4 N
Radius of front wheel	R_f	0.18 m
Radius of rear wheel	R_r	0.22 m
Height of front axle	H	0.20 m
Height CG from ground	h	0.17 m
Inclination angle	θ	13.36 %
Distance of CG above the axle plane	(h-r)	0.01 m
Permanent magnet synchronous in-wheel motor		
DC voltage source	V_{dc}	48 V
Number of poles pairs	P	22
d-axis inductance	L_d	0.0066 H
q-axis inductance	L_q	0.0058 H
PMs flux	ψ_f	0.175 Wb
Moment inertia of the wheel	J	0.00176 $Kg.m^2$
Viscous damping	B	0.00038818 Nms^{-1}
Stator resistance	R_s	1.4
Load torque	T_L	1
Vehicle control parameters		
Proportional gain	k_p	700
Integral gain	k_i	6
Derivative gain	k_d	180
Inner-loop control parameter		
Proportional gain	k_p	10
Integral gain	k_i	8

3.0 CONTROL STRATEGY

Figure 5 shows the anti-slip-based wheel velocity control strategy for the IWM-EV. Following the idea from the original research done by [68], here X is the reference velocity which calculated vehicle velocity (v_x) as $\frac{1}{r(1-\lambda)}$ generalized from (16), with the assumption that the vehicle operates in the acceleration mode when $\omega R_w > v_x$ and λ be the desired slip ratio of 0.2. In addition, vector K is the throttle pedal-to-torque ratio for distributing the torque command T_{cmd} to the driving wheels, where K is described as $0 < K < 100\%$.

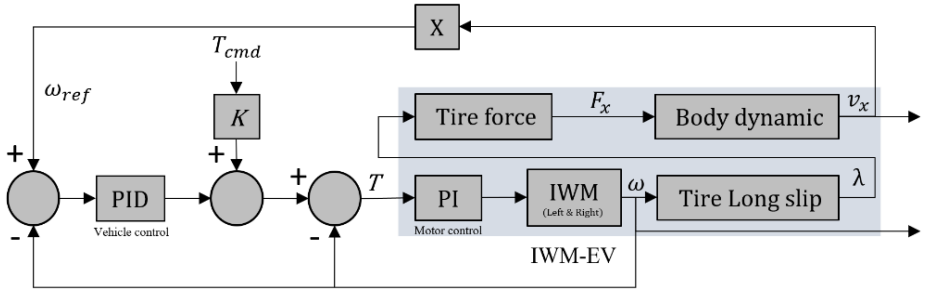

Figure 5. IWM-EV control strategy

4.0 SIMULATION AND EXPERIMENTAL RESULTS

In order to test the IWM-EV along with its control scheme, a series of simulations and experimental work have been carried out. The test used in this study was acceleration tests, acceleration then braking test on level pavement, and road gradient tests that generalized from SAE Standard J1666-199908. In this stage, it was targeted to execute the experimental work in three different speed limit conditions, which are 10, 15, and 20 km/h. However, due to the track limit, which has a maximum distance of about 150 meters, the simulation and experiment are restricted to the speed range of 15 and 20 km/h, corresponding to the speed limit authorized in the campus vicinity. This is owing to the fact that a greater distance is necessary to attain and sustain a vehicle speed exceeding 20 km/h.

Additionally, the incapability of the IWMs to attain high-speed dynamics within the available distance precludes the validation of the 30 km/h speed tests. On the other hand, the road gradient acceleration was done at a speed of only 20 km/h. It is worth noting that the IWMs capacity used in the vehicle is a 1 kW three-phase motor, and the location of the track where the experimental tests were conducted is shown in Figure 6. Several behaviours have been observed: vehicle speed, wheel speed, distance travel, battery voltage, current, and driving torque provided by the IWMs. The results are shown in Figures 9, 10, and 11, respectively, where the solid lines represent the experimental data, while the dashed line represents the simulation responses. Note that all the experimental data were filtered using (lowpass).

Figure 6. Route used to run the experimental tests

4.1 Acceleration Tests on the Level Pavement at 10 km/h

The graph depicted in Figure 7 matches the results of an IWM-EV simulation model with the experimental results obtained on a level pavement. For clarity and comprehension, each of the figures presented below has been divided into three sections, illustrating the vehicle's acceleration, uniform velocity, and deceleration phases. These distinct phases of vehicle dynamics occur during different time intervals, which are $7.0 \leq t(s) \leq 9.0$, $9.0 \leq t(s) \leq 23.26$, and $23.26 \leq t(s) \leq 26.25$. In Figure 7(a), the throttle input gradually increased from minimum to maximum, causing the vehicle body to accelerate. Figure 7(b) shows that the vehicle body achieves a constant speed of 10 km/h. The vehicle body and wheel speed are nearly identical to the simulation and experiment, but there is a slight delay of approximately 0.01 seconds in the vehicle body speed due to the vehicle's inertia and load transfer from front to rear during acceleration. The vehicle's maneuver results in a distance travelled of 3.04 m from the initial state. If further refined, the vehicle's dynamic at acceleration is influenced by the electrical dynamic of the IWM system, where the throttle input given to the controller increases the IWM current of the controller to generate IWM speed. The controller produces a current from 1.68 A to 20 A, and the IWM current can be used to estimate the electromagnetic torque of the IWM. The torque produced ranges from 9.63 to 115.4 Nm. As the IWM current increases, there is a voltage drop of approximately 5% from the operating voltage of 48.0 V, with the maximum voltage drop occurring at the highest current.

Besides the second stage refers to the electric vehicle attaining a uniform speed of 10 km/h. To maintain this speed, the throttle input decreases linearly from 100% to 30%, and the vehicle covers a distance travel of 39.56 m. By referring to the dynamic electrical side in this stage, the maximum IWM current and estimated torque decrease linearly from 20.0 A to 5.72 A and 115.4 to 32.69 Nm, respectively. These changes in current also affected the voltage source, resulting in increased stability once the vehicle reached a uniform speed. On the other hand, the last stage alludes to the IWM-EV deceleration, where the throttle pedal is fully released, and the maximum braking input is applied, which causes the vehicle body and wheel speed to reduce drastically. The dissimilarity observed in the body and wheel speed was attributed to the incapability of the simulation to represent the exact situation faced by the real vehicle. This is aggravated by the use of low-cost sensors that generate noise and are sensitive to the rough pavement, where the MRAE value for body and wheel speed was 0.37 % and 0.22 %. In terms of distance travel, the stopping distance upon the vehicle stop is 7.95 m

from the point of deceleration, which was affected by both the vehicle's inertia and load transfer from rear to front. It can be seen that the simulation result is able to replicate the pattern of the experimental data, which shows the highest similarity with an MRAE error of 0.14 %.

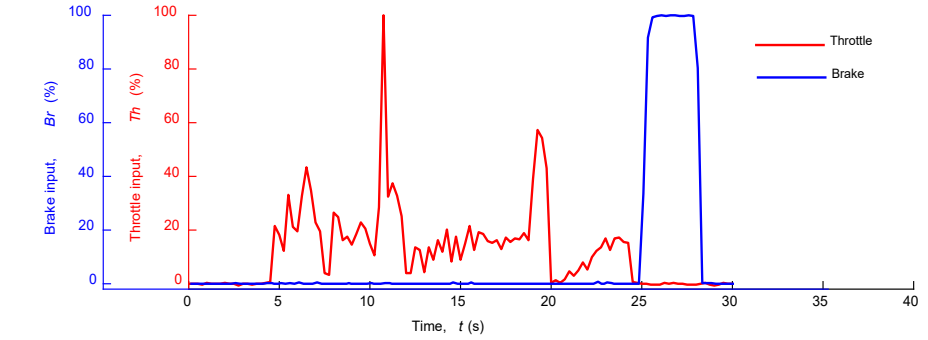

(a)

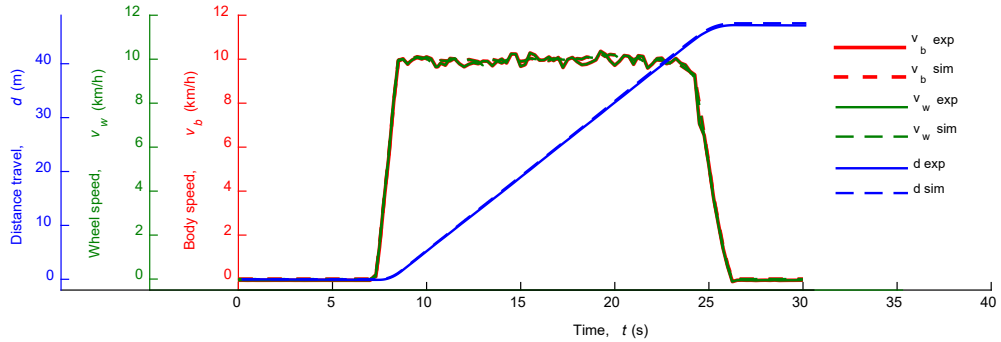

(b)

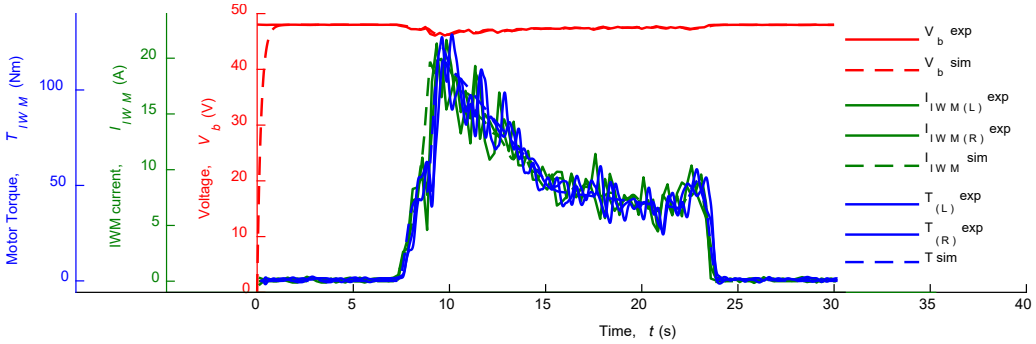

(c)

Figure 7. The evaluation of IWM-EV acceleration performance on the level pavement at 10 km/h: (a) throttle and braking input; (b) dynamic vehicle characteristics; (c) electrical dynamic characteristics

On the dynamic electrical side, it also can be observed that both the IWM current and estimated torque are minimized, while the voltage supplied to the IWM system remains stable at its operational level. Focusing on the IWM current and torque, there is a difference between the simulation and experiment, as well as the amplitude of both sides of the IWM current and torque, even though it utilized the same power source to operate the IWM system. There are two factors that contribute to the differences, which are mechanical-electrical analogies. Mechanically, there is subtle friction on the disc brake due to the uneven brake pad's grip on both sides of the brake. Meanwhile, in terms of electrical, it is caused by using longer power wires to obtain the power source on the right side, compared to the left side. This leads to imbalanced resistance on both systems, resulting in a higher IWM current on the right side to attain the desired speed. Specifically, the MRAE values of IWM current obtained on the left and right sides are 2.01% and 2.03%, while for IWM torque, the MRAE values on the left and right sides are 2.34 % and 2.37 %, respectively. In terms of the battery voltage, there is a difference at the initial and bottom peaks of the voltage drop between the simulation and experiment. The simulation begins reading the voltage from its lowest to its operating value, resulting in a delay of 1.1 seconds at the initial peak. Besides, the variation between the simulation and experiment at the bottom peak of the battery voltage is caused by the noise produced during the experiment, where the MRAE value of the battery voltage is 0.31 %.

To ensure the reliability of the IWM-EV controller, this study is continued by conducting the tests at varying speeds of 15 and 20 km/h, as seen in Appendix A. Although both tests have shown similar behavioural characteristics with the 10 km/h tests, there are variations in amplitude and MRAE value. According to Table 2, the MRAE values for speeds of

15 and 20 km/h are comparable to those at 10 km/h and still within the acceptable range of error. According to Hudha [59], the essential characteristic of a control-oriented model is the trend of the simulation. The results can be agreed upon as long as the simulation trend is closely similar to the experimental data with acceptable deviations and errors. Aside from that, Rykiel [60] has mentioned that the acceptable level of deviation between experimental data and simulation response is below 5 % of disparities. According to Ahmad [26], 5% disparities are the maximum acceptable error in expressing the credibility of a simulation. Therefore, based on these statements, it can be confirmed and concluded that the IWM-EV model simulation and its control scheme are realistic. It is worth noting that, as previously explained, the MRAE value of IWM current and torque is higher on the right side than the left side due to mechanical-electrical analogies.

Table 2. MRAE of acceleration performance tests on the level pavement at 10, 15, and 20 km/h

Speed (km/h) / Parameter	MRAE (%)		
	10	15	20
Vehicle body speed, v_b	0.37	0.33	0.43
Wheel speed, v_w	0.22	0.27	0.20.
Distance travel, d	0.14	0.11	0.16
Battery voltage, V_b	0.31	0.33	0.43
Left IWM current, I_{IWM}	2.01	2.02	2.07
Right IWM current, I_{IWM}	2.03	2.17	2.10
Left Torque motor, T_{IWM}	2.34	2.02	2.17
Right Torque motor, T_{IWM}	2.37	2.23	2.27

4.2 Acceleration, then Braking Tests on the Level Pavement at 10 km/h

In this test, the IWM-EV was driven to reach the target speed from rest, and a sudden braking input was then applied to halt the wheel's rotation and drastically reduce the body speed. Once the vehicle stopped, the sudden throttle input was applied to make the vehicle accelerate again. Figure 8 shows the validation results of the acceleration and braking tests at 10 km/h. Figure 8(a), 8(b), and 8(c) represent the throttle and braking input applied to the vehicle, demonstrating the vehicle dynamics and the dynamic electrical response, respectively. In order to ease the understanding of this outcome, the validation results have been categorized into five parts: vehicle accelerating, vehicle maintaining the target speed, vehicle applying a sudden braking input, vehicle applying sudden throttle input, and vehicle stopping. Noted that, in order to enhance the confidence of the experimental results, the tests were conducted repeatedly about three sets for each case. Focusing on Figure 8(a), the maximum throttle input was given at 3 s, which then initiated the wheel to rotate and thus made the vehicle speed up to 10 km/h. It is noticed that within 4.61 s, the vehicle speed was able to reach about 10 km/h, which covered a distance travel of 8.44 m. At this point, a high current was generated at both of the IWMs, which were 19.90 A, providing the IWMs torque about 115.4 Nm, respectively. This high current generally causes the battery voltage to drop and gradually reduce as the vehicle gets closer to the target speed, reflecting the effect of inertia on the vehicle.

On the other hand, at the second stage, which was $7.61 \leq t(s) \leq 13.87$, the throttle applied was determined by how swiftly the wheel and body reached their desired speed. Even so, it was challenging for the drivers to maintain this speed over time due to various factors such as road surface, road incline, obstacles on the road, the impact of inertia, and wind resistance. As a result, there were slight deviations from the target speed, but it was still within the acceptable range. On the dynamic electrical side, it can be observed that the current generated by the IWM decreased from 19.76 A to 8.81 A, along with a reduction in IWM torque from 114.2 Nm to 50.83 Nm. The reduction of the current usage to a minimum value during maneuver has brought positive ramifications to the battery voltage as it remains optimal and thus experiences a minimal voltage drop. In addition, the next stage refers to the time range of $13.87 \leq t(s) \leq 15.67$, where the throttle input is released at 13.87 s, while the brake input is abruptly applied at 14.0 s until the wheel and body completely stop. Here, the vehicle took 1.67 s to stop entirely at 15.67 s while the stopping distance experienced was 1.5 m. Throughout this period, both sides' IWMs' current decreased to its minimum operating current of 1.6 A. In this condition, the battery voltage reverts to its operational level of 48 V because the IWM-EV was totally stopped from rotating and influenced by external disturbances.

An extension from the last stage, the vehicle was reaccelerated until 24.75 s. At this point, sudden full throttle input was applied to the vehicle, causing the IWM-EV to accelerate from static to 14.57 km/h, resulting in IWM-EV travelling a distance of 21.51 m. Looking on the dynamic electrical side, there is an increment in the IWMs current and electromagnetic torque to a maximum of 20.0 A and 115.4 Nm, respectively. The significant increment in current induces the battery voltage to drop a maximum of 45.96 V @ 5 % from its operating level. After that, sudden braking was applied at 24.75 s, making the vehicle stop completely at 2.25 s later. When comparing the simulation and experimental results, it is noticed that there is a high percentage of similarity between them. It can be seen in the MRAE values for wheel and body speeds were 1.20 % and 1.37 %, respectively. It is worth knowing that the vehicle's stopping distance is 2.93 m from its deceleration point, demonstrating 0.17 % disparities between the simulation and experiment. Concentrating on the dynamic electrical perspective, it can be seen that all parameters, including IWMs current, torque, voltage, and control strategy, are reliable in the simulation system, making that the differences between simulations and experimental data are

less than 2.5 %, such as figured in MRAE value of current, torque and voltage were 2.17 %, 2.13 %, and 0.30 % respectively.

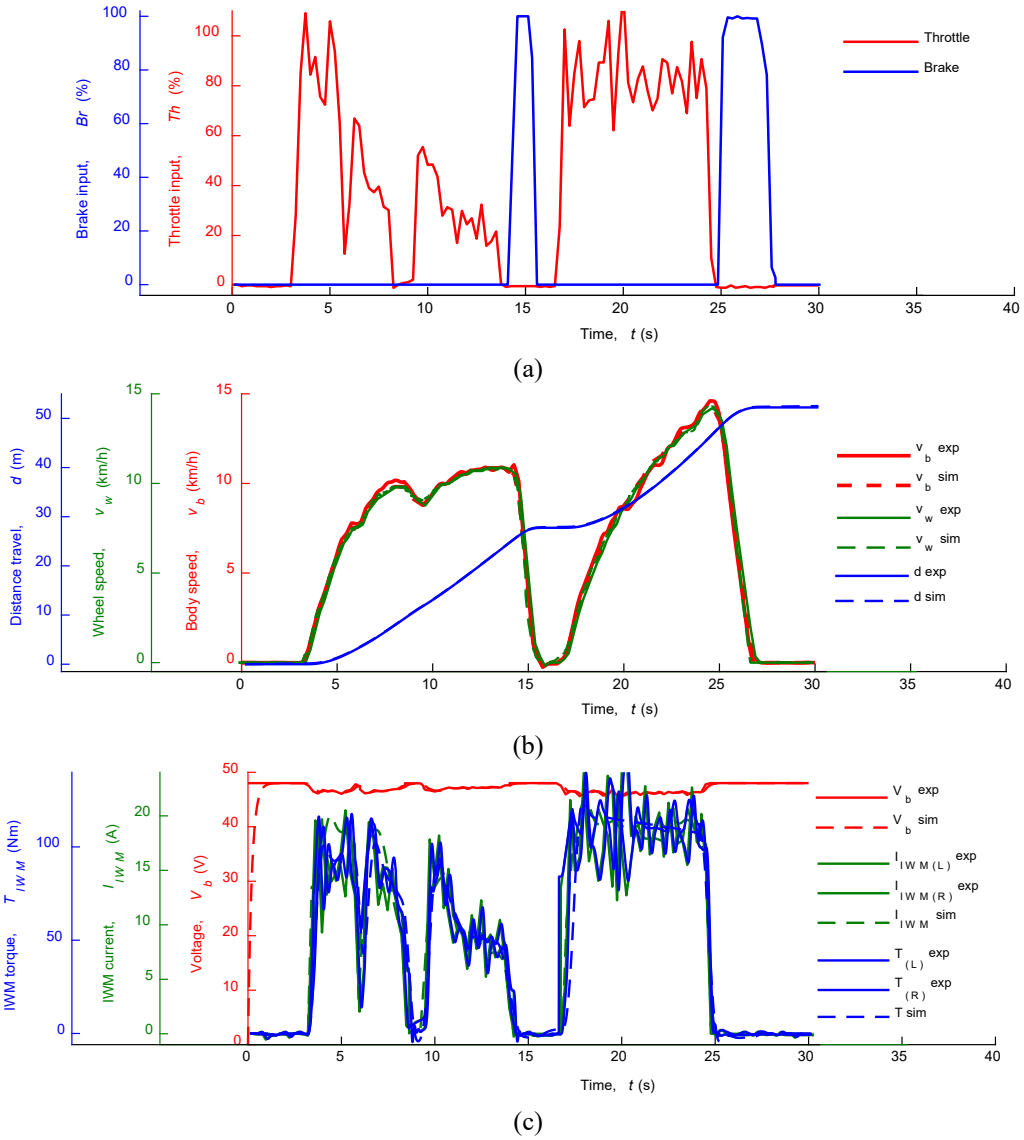

Figure 8. The evaluation of IWM-EV acceleration then braking performance on the level pavement at 10 km/h: (a) throttle and braking input, (b) dynamic vehicle characteristics and (c) dynamic electrical characteristics

In order to verify the credibility of the simulation and experimental data, other tests have been performed at different speeds, which are 15 and 20 km/h. The simulation and experiment results are shown in Figures 12 and 13 in Appendix B, while the MRAE values for each test are listed in Table 3.

Table 3. MRAE of acceleration, then braking tests on the level pavement at 10, 15, and 20 km/h

Parameter \ Speed (km/h)	MRAE (%)		
	10	15	20
Vehicle body speed, v_b	1.37	1.40	1.33
Wheel speed, v_w	1.20	1.03	1.70
Distance travel, d	0.17	0.49	0.20
Battery voltage, V_b	0.30	0.27	0.23
Left IWM current, I_{IWM}	2.03	2.10	2.13
Right IWM current, I_{IWM}	2.17	2.40	2.20
Left Torque motor, T_{IWM}	2.10	2.13	2.23
Right Torque motor, T_{IWM}	2.13	2.17	2.27

4.3 Road Gradient Tests at 10 km/h

To delve deeper into the veracity of the vehicle model, another assessment was performed utilizing inclination road profiles. All of the vehicle characteristics during the performance tests are presented in Figure 9. Figure 9(a) presents the input given by the driver, Figure 9(b) illustrates the IWM-EV dynamic characteristic, while Figure 9(c) demonstrates the

electrical dynamic of the vehicle. The figure can be comprehended by dividing the total 45.0 seconds of dynamic tests into four segments: vehicle acceleration, vehicle maintaining the target speed, vehicle ascent on a gradient road, and vehicle reaching the top of the gradient road. The time taken for those segments are classified into the four-time interval, which are $3.25 \leq t(s) \leq 10.4$, $10.4 \leq t(s) \leq 31.15$, $31.15 \leq t(s) \leq 35.08$ and $35.08 \leq t(s) \leq 45.00$ respectively.

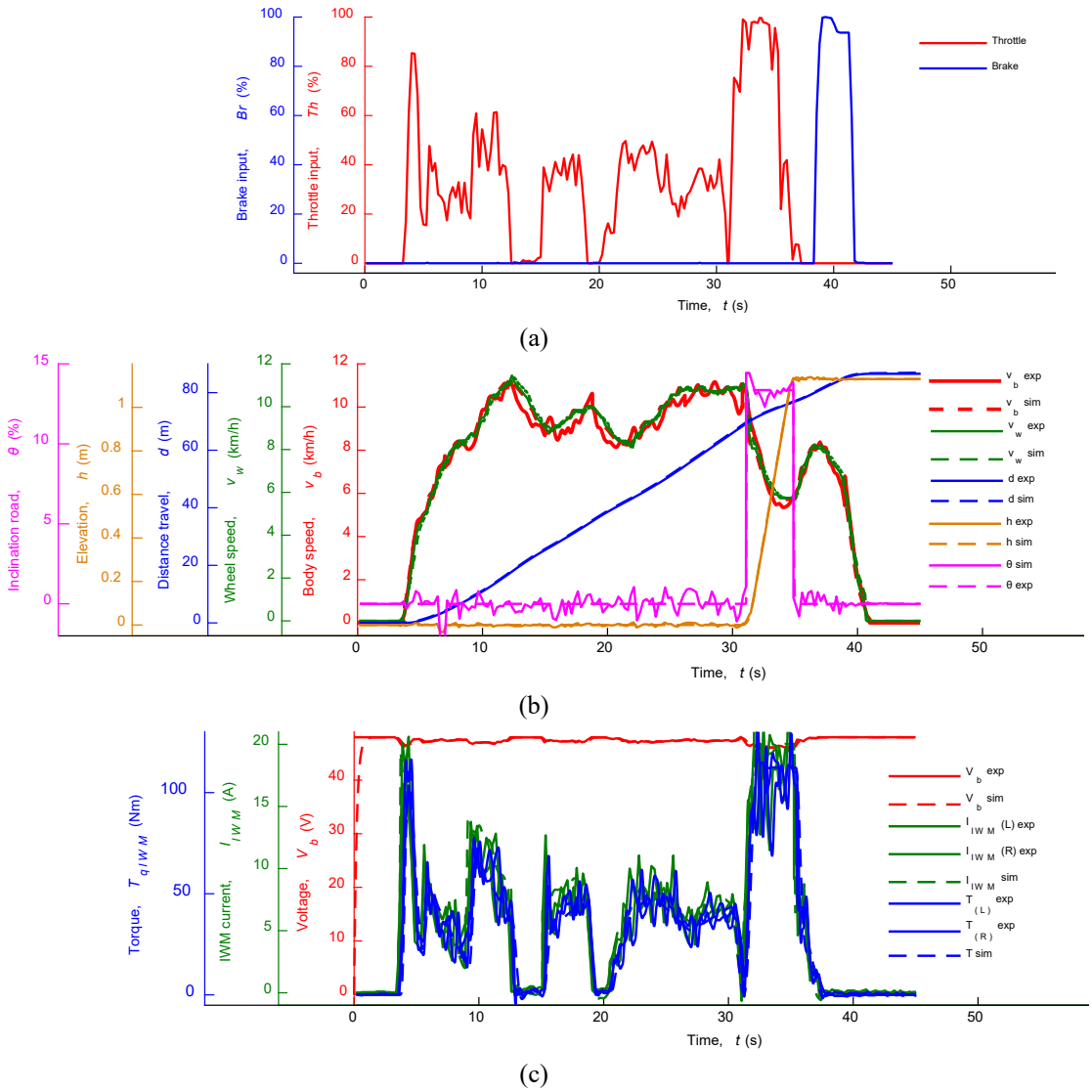

Figure 9. The evaluation of IWM-EV acceleration performance on incline road at 10 km/h: (a) throttle and braking input, (b) dynamic vehicle characteristics and (c) electrical dynamic characteristics

The tests begin at the acceleration state, where the driver gives the throttle input to reach the intended speed. In this condition, it is seen that the peak value of throttle input is 85.33 % at the first 4.0 s, followed by 47.65 % at 5.5 s and 60.88 % at 9.5 s, which can be seen in Figure 9(a). The applied throttle input has resulted in the vehicle's wheel and body starting to maneuver from stationary to the target speed of 10 km/h, which can be depicted in Figure 9(b). The maneuverer of the vehicle in this time range leads to a distance travel of 12.58 m from its initial conditions. Besides, Figure 9(c) illustrates the electrical behavior of IWMs during acceleration, where the current and torque applied at both sides of the wheel at 4.0 s are 19.2 A and 110.2 Nm, respectively. The increment of the current causes the voltage drops due to the high current required to initiate wheel rotation, which is influenced by the body's inertia from the initial position.

The second stage refers to the vehicle maintaining a 10 km/h target speed. To achieve this, the throttle input is varied to ensure that the speed remains consistent even though it is hard for the driver to maintain the throttle input to achieve the intended speed. However, the percentage of throttle input applied depends on the target speed. When the vehicle speed exceeds the target, the throttle input is reduced, and conversely, when the speed is below the target, the throttle input is increased. The effect of this throttle input can be seen on the body and wheel speed, where the speed range is about 10 km/h with a maximum deviation of 17 %.

Regarding distance travel, the vehicle's maneuver in this stage covers a distance travel of 57.41 m. Apart from that, during this stage, the IWMs generate a current of 15.25 A, producing the IWM's torque of 68.72 Nm. Despite the high current, the percentage of voltage drop from its operating voltage of 48.0 V is only 1.35 % or 0.65 V. The lower voltage

drop is owing to the vehicle having attained the desired speed, which consequently reduces the impact of inertia on the vehicle. The following stage involves the vehicle starting to ascend an inclined road, which takes 3.92 seconds to climb completely with maximum throttle input. The inclination road has a slope and elevation of 13.36 % and 1.13 m from its base, respectively. A comparison between the simulation and experiment reveals that the elevation and incline road angle have a deviation of 0.12 % and 0.89 %, respectively. This discrepancy was not only caused by the noise generated from the accelerometer and gyroscope transducer MPU 6050, but also by the vehicle's vibration during maneuverer on the level pavement, which has a rough surface. During the period, the IWMs generate maximum current and torque of 19.93 A and 115.4 Nm, respectively, thus causing a voltage drop of 3.83 % from its operating voltage.

Aside from that, the final stage alludes to the vehicle reaching level pavement on the top of a gradient road, where the maximum braking input was applied and completely stopped at 40.64 s. Here, it is observed to have differences between the simulation and experiment of the wheel and body speed that has been analyzed, where the MRAE values are 3.93 % and 4.15 %, respectively. This is because the experimental tests experienced parasitic loss while the simulation merely simulated the model based on the given parameter. In retrospect, the time taken for the vehicle to stop completely is 2.39 s, where it is stemming from the load transfer of the vehicle from the rear to the front, which yields a stopping distance of 2.68 m. Notwithstanding, there is a small deviation in the distance travel, which is 0.11 %, owing to the simulation result being faster than the experimental data. The simulation and experimental data comparison found that the MRAE value of IWMs current, torque, and voltage were 1.36 %, 1.44 %, and 0.23%, respectively. These errors are due to the noise generated by the sensors and other electrical components, where electromagnetic interference occurs between the power and signal wire during the experiment. Therefore, there is a significant disparity between the data obtained from the experiment and the simulation results.

To bolster the confidence in the controller's performance on gradient road tests, the vehicle was tested at two different speeds of 15 and 20 km/h, as shown in Figure 14 and Figure 15, which can be seen in Appendix C. Generally, simulation results and experimental data exhibit similarities, where the error for each test was below 5 % and lay within the allowable spectrum, as seen in Table 4.

Table 4. MRAE of acceleration performance tests on incline roads at 10, 15, and 20 km/h

Speed (km/h) / Parameter	MRAE (%)		
	10	15	20
Vehicle body speed, v_b	4.15	0.27	0.34
Wheel speed, v_w	3.93	0.18	0.23
Distance travel, d	0.11	0.15	0.14
Elevation, h	0.12	0.14	0.15
Inclination road, θ	0.89	0.62	0.57
Battery voltage, V_b	0.23	0.21	0.29
Left IWM current, I_{IWM}	1.36	1.33	1.69
Right IWM current, I_{IWM}	1.36	1.33	1.69
Left Torque motor, T_{IWM}	1.44	1.49	1.80
Right Torque motor, T_{IWM}	1.44	1.49	1.80

5.0 CONCLUSIONS

In this study, a 5-DOF in-wheel motor-based electric vehicle model has been developed in MATLAB Simulink software by using PID based controller [28] as the vehicle longitudinal control strategy. In order to authenticate the efficacy of the simulation model, validation tests have been made by using an instrumented experimental IWM-EV, which has been developed in the Autotronic Laboratory, Faculty of Mechanical Engineering, UTeM. Several transducers and data acquisition systems were installed in the vehicle, including an Arduino UNO R3, current sensor, hall sensor, brake sensor, voltage sensor, encoder, and gyroscope MPU 6050. Various dynamic tests were conducted namely acceleration tests, acceleration then braking tests, and road gradient tests at the speed of 10, 15, and 20 km/h, respectively. Various vehicle dynamic and electrical behaviour have been analyzed, including wheel speed, body speed, distance travel, battery voltage, IWM current, and motor torque. In accordance with the verification data, it can be seen that the response of the IWM-EV simulation model is similar to the experimental vehicle with less than 5 % error. The deviation between simulation and experimental data is generally contributed by the driver's challenge in maintaining a uniform speed during maneuvering and the neglection of the road surface irregularity in the simulation scheme. As mentioned by Ahmad et al. [26], the primary feature of a control-oriented model is the pattern of the model's response. As long as the model's response pattern closely resembles the measured response with an acceptable level deviation of error, the results can be deemed reliable. Apart from that, Rykiel has stated that the allowable level of difference between the measured and simulated responses should be less than 5%, as well as Sergent who considers this margin as the highest allowable error to establish the credibility of a simulation. Hence, based on this statement, it can be inferred that the simulation model and control strategy are sufficient and reliable and can be used to develop advanced electric vehicle technology in the next research study by employing a stand-alone microcontroller that is more sophisticated, with higher signal transmission speed and stability, such as Votol 7280 and LAUNCHXL-F28379D.

The development process, the controller implementation, and the conducted testing can be seen in this video: https://www.youtube.com/watch?v=Q5SrJY5Opfs

6.0 ACKNOWLEDGEMENT

This work is a part of a research project entitled "Reliability Test of Electronic Wedge Brake (EWB) As Advance Emergency Braking System in Semi-Autonomous In-Wheeled Motor Based Electric Vehicle", funded by PJP grant (PJP/2022/ FTKEE/S01879) lead by Ts. Dr. Mohd Hanif Che Hasan, and continuation from the previous research project "Characterization of brake force and wedge properties of IBS based electronic wedge brake for autonomous braking system," funded by PJP grant (PJP/2020/FKM/PP/S01783) lead by Ir. Ts. Dr. Fauzi bin Ahmad.

7.0 REFERENCES

[1] R. M. Salgado, F. Danzi, J. E. Oliveira, A. El-Azab, P. P. Camanho, and M. H. Braga, "The latest trends in electric vehicles batteries," *Molecules*, MDPI AG. vol. 26, No. 11, pp. 1–41, 2021.

[2] J. A. Sanguesa, V. Torres-Sanz, P. Garrido, F. J. Martinez, and J. M. Marquez-Barja, "A review on electric vehicles: technologies and challenges," *Smart Cities*, MDPI, vol. 4, No. 1, pp. 372–404, 2021.

[3] S. Parmar and M. Patel, "A review on renewable energy integration for electric vehicles," *International Journal of Engineering Applied Sciences and Technology*, vol. 5, no. 8, pp.247-254, 2020.

[4] K. Nęcka and J. Knaga, "Environmental impact assessment for electric vehicles," *IOP Conference Series: Earth and Environmental Science*, vol. 1782, no. 1, pp.1-5, 2021

[5] M. R. Wahid, B. A. Budiman, E. Joelianto, and M. Aziz, "A review on drive train technologies for passenger electric vehicles," *Energies (Basel)*, vol. 14, no. 20, 2021.

[6] B. Li, H. Du, and W. Li, "A potential field approach-based trajectory control for autonomous electric vehicles with in-wheel motors," *IEEE Transactions on Intelligent Transportation Systems*, vol. 18, no. 8, pp. 2044–2055, 2017.

[7] S. A. Bagloee, M. Tavana, M. Asadi, and T. Oliver, "Autonomous vehicles: challenges, opportunities, and future implications for transportation policies," *Journal of Modern Transportation*, vol. 24, no. 4, pp. 284–303, 2016.

[8] W. Xu, H. Chen, H. Zhao, and B. Ren, "Torque optimization control for electric vehicles with four in-wheel motors equipped with regenerative braking system," *Mechatronics*, vol. 57, pp. 95–108, 2019.

[9] S. Ding and J. Sun. "Direct yaw-moment control for 4WID electric vehicle via finite-time control technique," *Nonlinear Dynamics*, vol. 88, no. 1, pp. 239–254, 2017.

[10] L. de Novellis, A. Sorniotti, and P. Gruber, "Driving modes for designing the cornering response of fully electric vehicles with multiple motors," *Mechanical Systems and Signal Processing*, vol. 64–65, pp. 1–15, 2015.

[11] B. M. Nguyen, H. van Nguyen, M. Ta-Cao, and M. Kawanishi, "Longitudinal modelling and control of in-wheel-motor electric vehicles as multi-agent systems," *Energies (Basel)*, vol. 13, no. 20, 2020.

[12] Y. Li, H. Deng, X. Xu, and W. Wang, "Modelling and testing of in-wheel motor drive intelligent electric vehicles based on co-simulation with Carsim/Simulink," *IET Intelligent Transport Systems*, vol. 13, no. 1, pp. 115–123, 2019.

[13] Z. Zhao, L. Zhang, J. Wu, L. Gu, and S. Li, "Vertical-longitudinal coupling effect investigation and system optimization for a suspension-in-wheel-motor system in electric vehicle applications," *Sustainability*, vol. 15, no. 5, p. 4168, 2023.

[14] O. P. Adeleke, Y. Li, Q. Chen, W. Zhou, X. Xu, and X. Cui, "Torque distribution based on dynamic programming algorithm for four in-wheel motor drive electric vehicle considering energy efficiency optimization," *World Electric Vehicle Journal*, vol. 13, no. 10, 2022.

[15] C. V. Pop, D. Fodorean, and D. C. Popa, "Structural analysis of an in-wheel motor with integrated magnetic gear designed for automotive applications," *Sustainability (Switzerland)*, vol. 14, no. 19, 2022.

[16] S. Tan, Y. Wang, W. Cheng, T. Luo, N. Zhang, *et al*., "Cascade direct yaw moment control for an independent eight in-wheel motor-driven autonomous vehicle," *Electronics (Switzerland)*, vol. 11, no. 18, pp. 1-11, 2022.

[17] G. Park, "A Vehicle Lateral Motion Control Based on Tire Cornering Stiffness Estimation Using In-Wheel Motors," *Electronics (Switzerland)*, vol. 11, no. 16, pp. 1-12, 2022.

[18] S. He, X. Fan, Q. Wang, X. Chen, and S. Zhu, "Review on torque distribution scheme of four-wheel in-wheel motor electric vehicle," *Machines*, MDPI, vol. 10, no. 8, 2022.

[19] C. Li, X. Guo, J. Fu, W. Fu, Y. Liu, *et al*., "Design and analysis of a novel double-stator double-rotor motor drive system for in-wheel direct drive of electric vehicles," *Machines*, vol. 10, no. 1, pp. 1-13, 2022.

[20] S. Kaushik, "Modelling and simulation of electric vehicle to optimize its cost and range," *International Journal of Engineering and Advanced Technology*, vol. 8, no. 6, pp. 415–419, 2019.

[21] T. Vo-Duy and M. C. Ta, "A signal hardware-in-the-loop model for electric vehicles," *ROBOMECH Journal*, vol. 3, no. 1, pp. 1-11, 2016.

[22] Y. Chung and Y. P. Yang, "Hardware-in-the-loop simulation of self-driving electric vehicles by dynamic path planning and model predictive control," *Electronics (Switzerland)*, vol. 10, no. 19, 2021.

[23] W. Sun, J. Rong, J. Wang, W. Zhang, and Z. Zhou, "Research on optimal torque control of turning energy consumption for EVs with motorized wheels," *Energies (Basel)*, vol. 14, no. 21, 2021.

[24] T. Feliciani , J. Luo, L. Ma, P. Lucas, F. Squazzoni, A. Marušić, K. Shankar, "A scoping review of simulation models of peer review," *Scientometrics*, vol. 121, no. 1, pp. 555–594, 2019.

[25] P. Li and H. Xu, "Braking efficiency and stability of chassis braking system of combine harvester: The theoretical derivation and virtual prototype simulation," *Mathematical Problems in Engineering*, vol 2019, no. 1, pp. 1-18, 2019.

[26] F. Ahmad, "Adaptive fuzzy fractional proportional integral derivative controller for antilock braking system using electronic wedge brake," Ph.D thesis, Universiti Teknologi Malaysia, Johor Bharu, 2017.

[27] F. Ahmad, K. Hudha, S. Mazlan, H. Jamaluddin, H. Zamzuri, *et al*. "Modelling and control of a fixed calliper-based electronic wedge brake," *Strojniski Vestnik/Journal of Mechanical Engineering*, vol. 63, no. 3, pp. 181–190, 2017.

[28] F. Ahmad, K. Hudha, S.A. Mazlan, H. Jamaluddin, V.R. Aparow, M.R.M. Yunos, "Simulation and experimental investigation of vehicle braking system employing a fixed calliper based electronic wedge brake," *Simulation: Transactions of the Society for Modeling and Simulation International 00(0)*, vol. 94, no. 4, pp.327-340.
[29] S. Mishra, M. Anurag, and S. Tomer, "Speed control of PMSM Drives by using neural network controller," *Advance in Electronic and Electric Engineering*, vol. 4, No. 4, pp. 353-360, 2014.
[30] A. Mora, A. Orellana, J. Juliet, and R. Cardenas, "Model predictive torque control for torque ripple compensation in variable-speed PMSMs," *IEEE Transactions on Industrial Electronics*, vol. 63, no. 7, pp. 4584–4592, 2016.
[31] M. S. Wang, I. N. Syamsiana, and F. C. Lin, "Sensorless speed control of permanent magnet synchronous motors by neural network algorithm," *Mathematical Problems in Engineering*, vol. 2014, pp. 1-7, 2014.
[32] Q. Liu and K. Hameyer, "Torque ripple minimization for direct torque control of PMSM with modified FCSMPC," *IEEE Transactions on Industry Applications*, vol. 52, no. 6, pp. 4855–4864, 2016.
[33] G. Han, W. Fu, W. Wang, and Z. Wu, "The lateral tracking control for the intelligent vehicle based on adaptive PID neural network," *Sensors (Switzerland)*, vol. 17, no. 6, 2017.
[34] L. Nie, J. Guan, C. Lu, H. Zheng, and Z. Yin, "Longitudinal speed control of autonomous vehicle based on a self-adaptive PID of radial basis function neural network," *IET Intelligent Transport Systems*, vol. 12, no. 6, pp. 485–494, 2018.
[35] H. C. Li, C. C. Lu, T. Eccarius, and M. Y. Hsieh, "Genetic algorithm with an event-based simulator for solving the fleet allocation problem in an electric vehicle sharing system," *Asian Transport Studies*. vol. 8, no. 2, pp. 1-10, 2022.
[36] Y. Zhu, K. Y. Lee, and Y. Wang, "Adaptive elitist genetic algorithm with improved neighbor routing initialization for electric vehicle routing problem," *IEEE Access*. vol. 9, no. 2, pp. 16661–16671, 2021.
[37] S. Karakatič, "Optimizing nonlinear charging times of electric vehicle routing with genetic algorithm," *Expert Systems with Applications,* vol. 164, no. 4, pp. 1-14, 2021.
[38] J. Zhao, Y. Ma, Z. Zhang, S. Wang, and S. Wang, "Optimization and matching for range-extenders of electric vehicles with artificial neural network and genetic algorithm," *Energy Conversion and Management,* vol. 184, no. 3, pp. 709–725, 2019.
[39] Z. Wang, Y. Liu, Z. Yang, and W. Yang, "Load frequency control of multi-region interconnected power systems with wind power and electric vehicles based on sliding mode control," *Energies (Basel)*, vol. 14, no. 8, 2021.
[40] K. Yang, D. Dong, C. Ma, Z. Tian, Y. Chang, and G. Wang, "Stability control for electric vehicles with four in-wheel-motors based on sideslip angle," *World Electric Vehicle Journal*, vol. 12, no. 1, pp.340-359, 2021.
[41] Y. Liang, Y. He, and Y. Niu, "Robust errorless-control-targeted technique based on MPC for microgrid with uncertain electric vehicle energy storage systems," *Energies (Basel)*, vol. 15, no. 4, 2022.
[42] M. Heydrich, V. Ricciardi, V. Ivanov, M. Mazzoni, A. Rossi *et al*. "Integrated braking control for electric vehicles with in-wheel propulsion and fully decoupled brake-by-wire system," *Vehicles*, vol. 3, no. 2, pp. 145–161, 2021.
[43] G. Tarchała and T. Orłowska-Kowalska, "Discrete sliding mode speed control of induction motor using time-varying switching line," *Electronics (Switzerland)*, vol. 9, no. 1, pp. 185-203, 2020.
[44] H. Wang, J. Han, and H. Zhang, "Lateral stability analysis of 4wid electric vehicle based on sliding mode control and optimal distribution torque strategy," *Actuators*, vol. 11, no. 9, 2022.
[45] W. Zhang, Z. Liu, and Q. Chen, "Electronic differential system based on adaptive smc combined with qp for 4wid electric vehicles," *World Electric Vehicle Journal*, vol. 12, no. 3, pp. 126-144, 2021.
[46] R. Pajer, A. Chowdhury, and M. Rodič, "Control of a multiphase buck converter, based on sliding mode and disturbance estimation, capable of linear large signal operation," *Energies (Basel)*, vol. 12, no. 14, pp. 2790-2816, 2019.
[47] Z. Sadeghi, M. Shahparasti, A. Rajaei, and H. Laaksonen, "Three-level reduced switch AC/DC/ac power conversion system for high voltage electric vehicles," *Sustainability (Switzerland)*, vol. 14, no. 3, pp. 1620-1635, 2022.
[48] Y. Wei, L. Sun, and Z. Chen, "An improved sliding mode control method to increase the speed stability of permanent magnet synchronous motors," *Energies (Basel)*, vol. 15, no. 17, pp. 6313-6327, 2022.
[49] G. A. Mendonça, D. P. V. Galo, L. C. M. Sales, B. J. Cardoso Filho, and T. A. C. Maia, "Design and experimental evaluation of an in-wheel flux-switching machine for light vehicle application," *Machines*, vol. 10, no. 8, pp. 671-689, 2022.
[50] J. Wideberg, C. Bordons, P. Luque, D. A. Mántaras, D. Marcos, and H. Kanchwala, "Development and experimental validation of a dynamic model for electric vehicle with in hub motors," *Procedia - Social and Behavioral Sciences*, vol. 160, pp. 84–91, 2014.
[51] C. M. Filho, D. F. Wolf, V. Grassi, and F. S. Osorio, "Longitudinal and lateral control for autonomous ground vehicles," *IEEE Intelligent Vehicles Symposium, Proceedings*. 2014, June, pp. 588–593.
[52] S. I. Haris, F. Ahmad, and A. K. M. Yamin, "Modelling and validation quarter vehicle traction model," In SA Conference Series: Industrial revolution 4.0. 2020, vol. 01, no. 01, pp. 65–73.
[53] B. Prasad Ganthia, S. Mohanty, S. Aparajita Pattanaik, and P. Kumar Rana, "Study of speed and torque characteristics of MATLAB-Simulink designed PMSM: A review," *International Research Journal of Engineering and Technology*, vol. 3, no. 3, pp. 731–734, 2016.
[54] M. H. C. Hasan, M. K. Hassan, F. Ahmad, M. H. Marhaban, and S. I. Haris, "A dynamic model of electronic wedge brake: experimental, control and optimization," *Indonesian Journal of Electrical Engineering and Computer Science*, vol. 23, no. 2, pp. 740–751, 2021.
[55] Mohd Hanif Che Hasan, Mohd Khair Hassan, Fauzi Ahmad, and Mohammad Hamiruce Marhaban, "Modelling and design of optimized electronic wedge brake," In International Conference on Automatic Control and Intelligent Systems (I2CACIS 2019). 2019, pp. 189-193.
[56] H. B. Pacejka and I. J. M. Besselink, "Magic formula tyre model with transient properties," *Vehicle System Dynamics*, vol. 27, No. 01, pp. 234-249, 1997.
[57] Gerdes. J. C., D. B. Maciuca, J. K. Hedrick, and Devlin, "Brake system modelling for ivhs longitudinal control. advance in robust and nonlinear control systems," In ASME Winter Annual Meeting, 1999, pp. 119-126.
[58] V. R. Aparow, "Fuzzy logic control of anti-lock braking system using electronic wedge brake mechanism," M.Sc thesis, Universiti Teknikal Malaysia Melaka, Melaka, 2013.
[59] K. Hudha, "Non-parametric modeling and modified hybrid skyhook groundhook control of magnetorheological dampers for automotive suspension system," Ph.D thesis. Universiti Teknologi Malaysia, Johor Bharu, 2005.
[60] E. J. Rykiel. "Testing ecological models: The meaning of validation," *Ecological Modelling*, vol. 90, no. 3, pp. 229–244, 1996.

8.0 APPENDICES

Appendix A

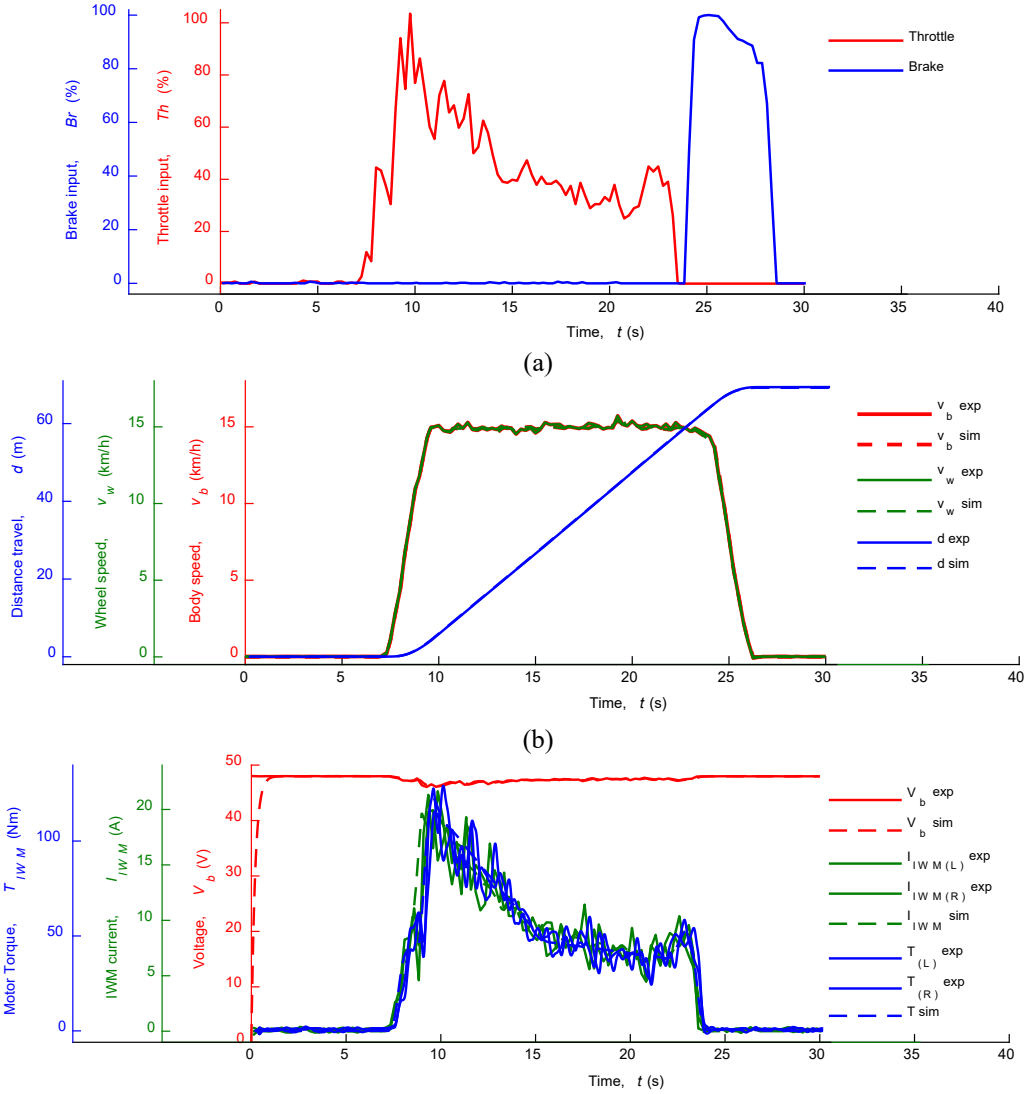

Figure 10. The evaluation of IWM-EV acceleration performance on the level pavement at 15 km/h: (a) throttle and braking input, (b) vehicle dynamic characteristics; (c) electrical dynamic characteristics

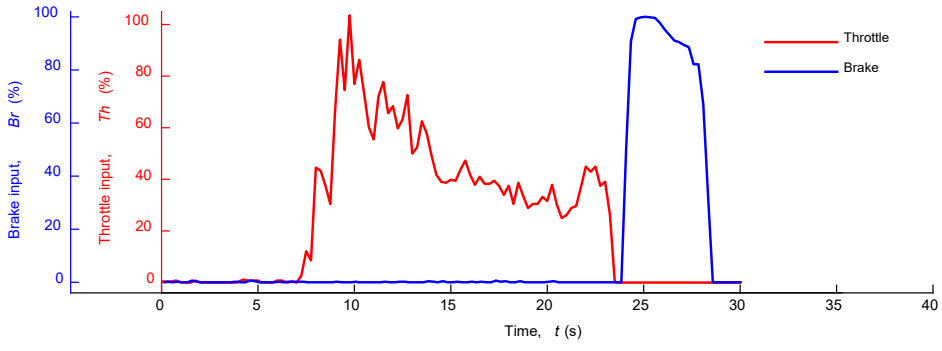

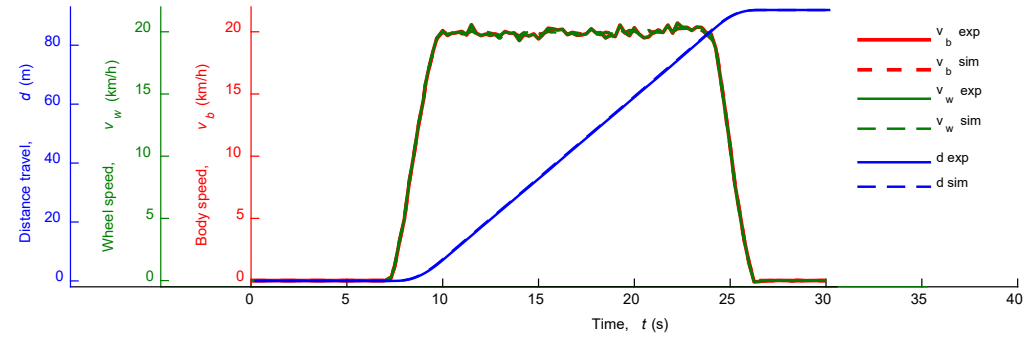

(b)

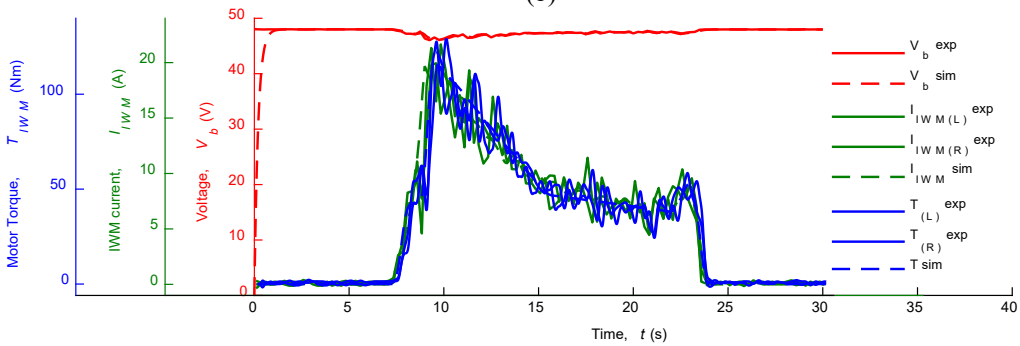

(c)

Figure 11. The evaluation of IWM-EV acceleration performance on the level pavement at 20 km/h: (a) throttle and braking input; (b) vehicle dynamic characteristics; (c) electrical dynamic characteristics

Appendix B

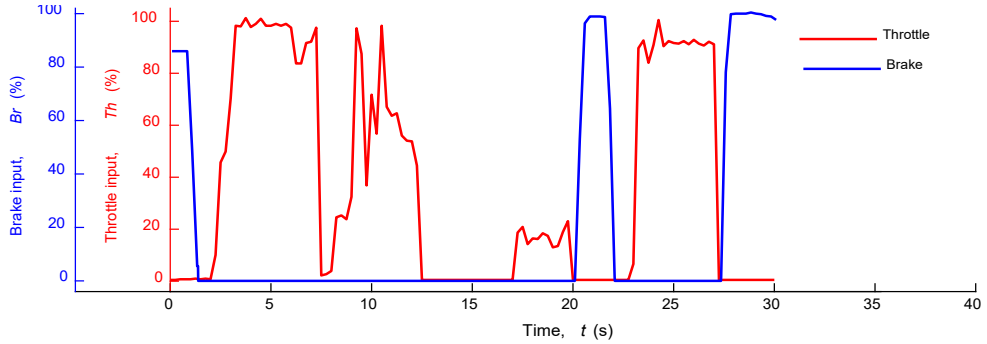

(a)

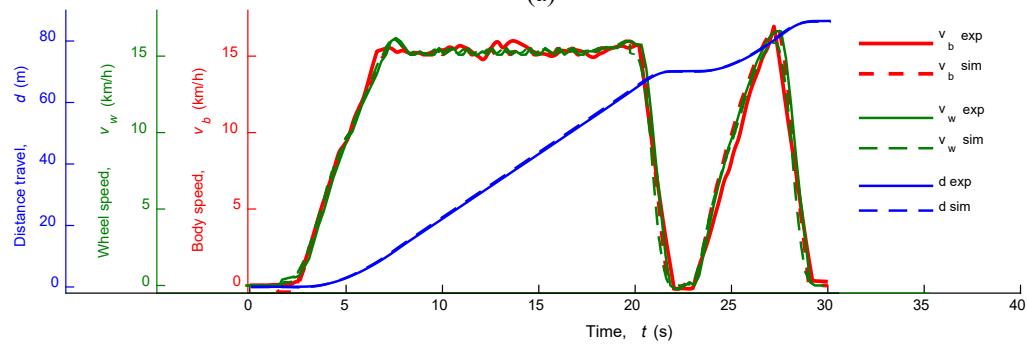

(b)

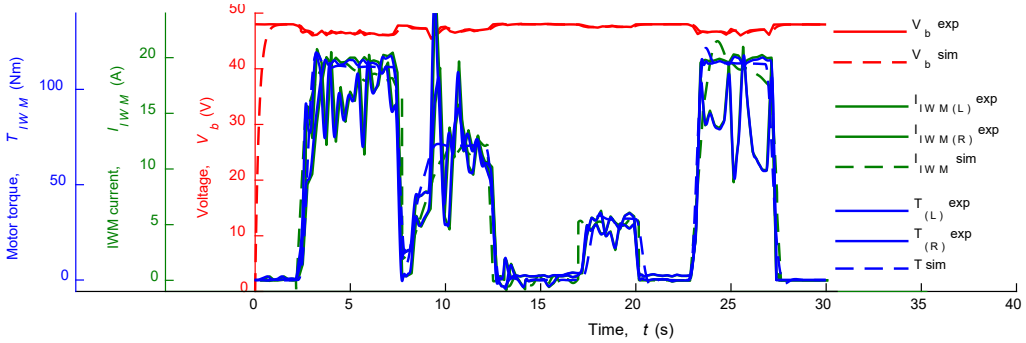

(c)

Figure 12. The evaluation of IWM-EV acceleration then braking performance on the level pavement at 15 km/h: (a) throttle and braking input, (b) vehicle dynamic characteristics and (c) electrical dynamic characteristics

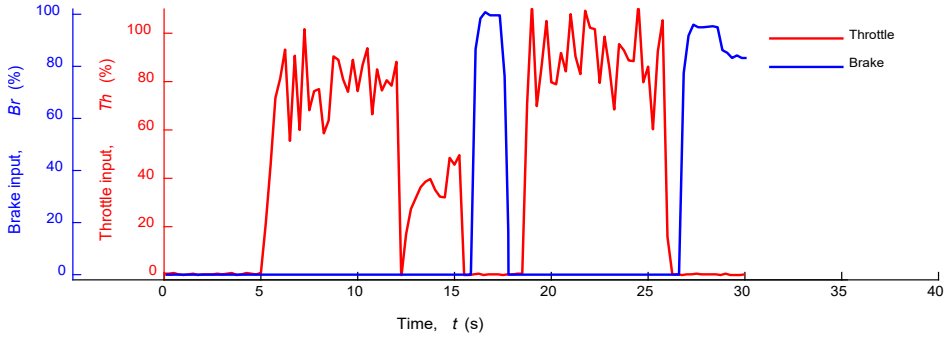

(a)

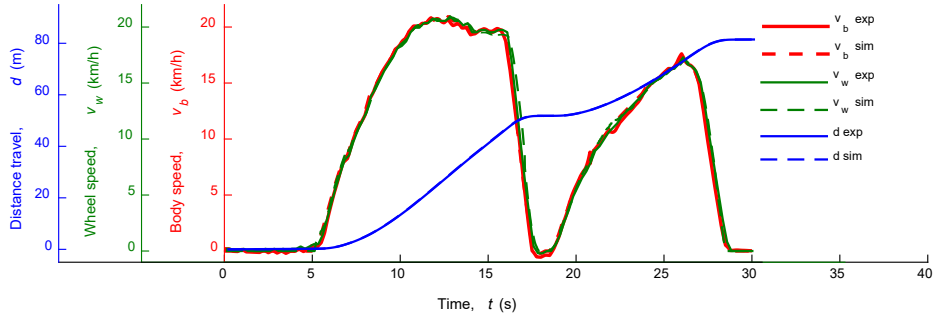

(b)

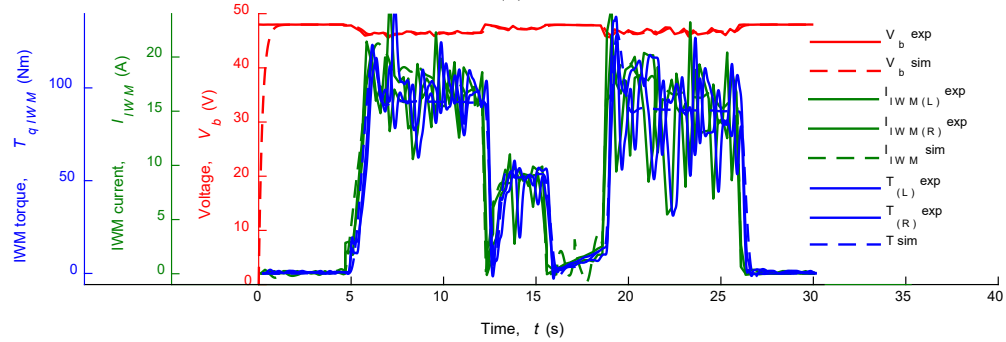

(c)

Figure 13. The evaluation of IWM-EV acceleration then braking performance on the level pavement at 20 km/h: (a) throttle and braking input; (b) vehicle dynamic characteristics; (c) electrical dynamic characteristics

Appendix C

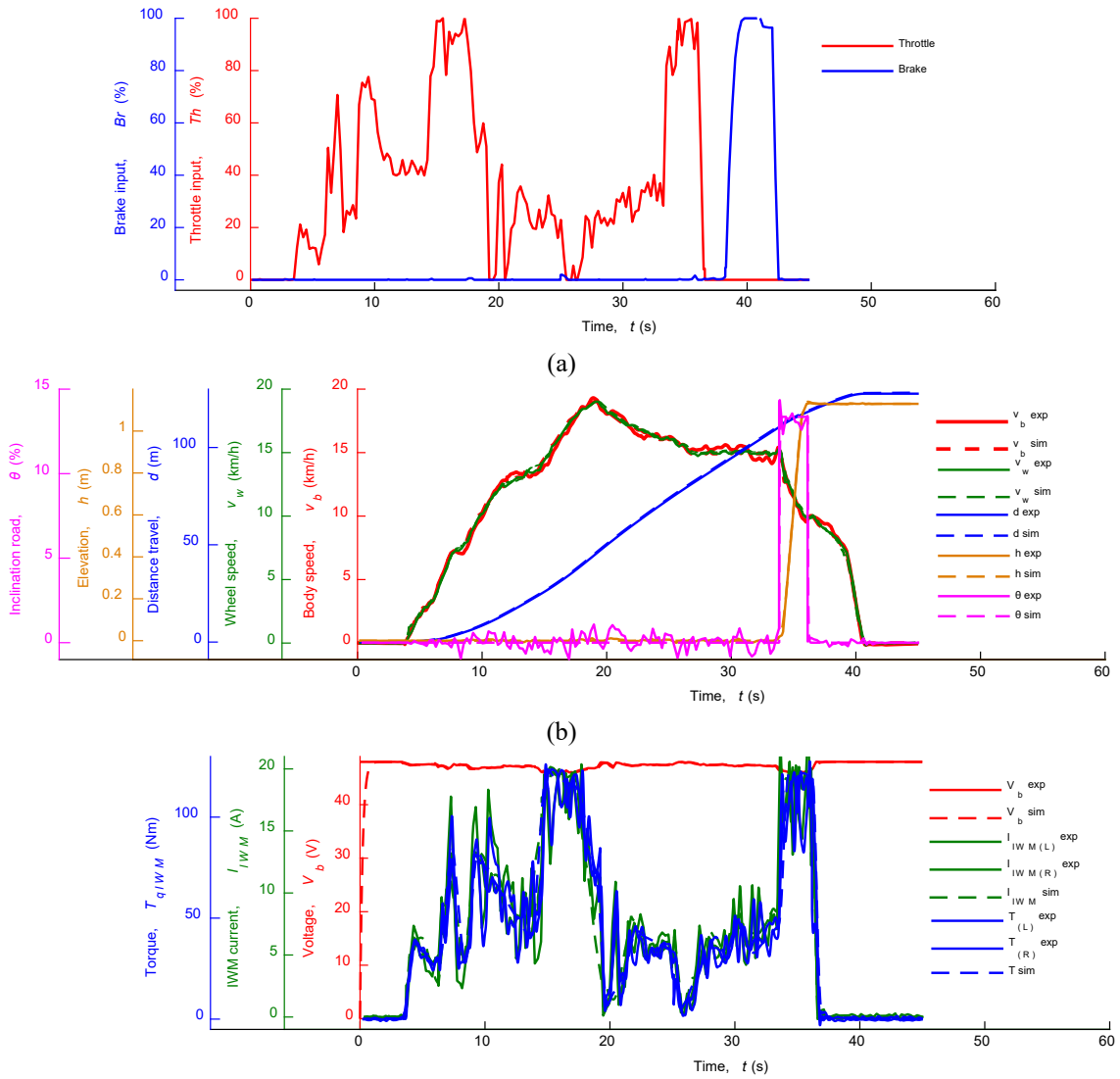

Figure 14. The evaluation of IWM-EV acceleration performance on incline road at 15 km/h: (a) throttle and braking input; (b) vehicle dynamic characteristics; (c) electrical dynamic characteristics

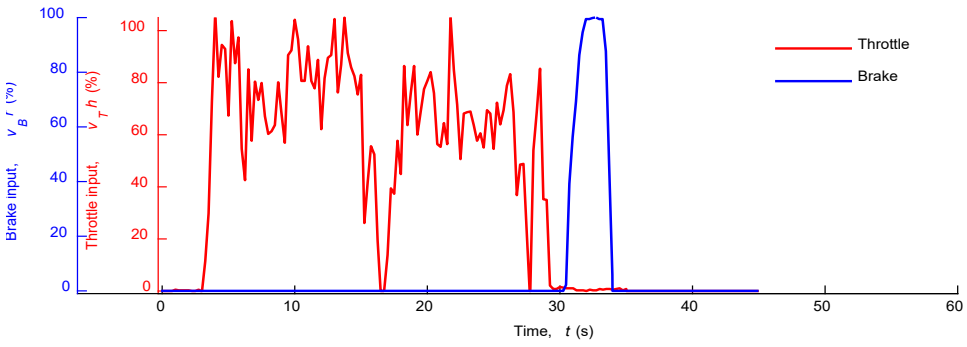

(a)

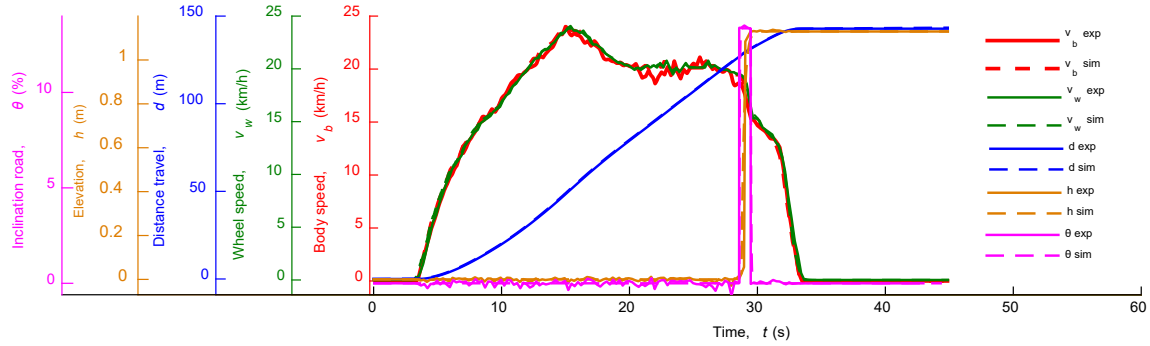

(b)

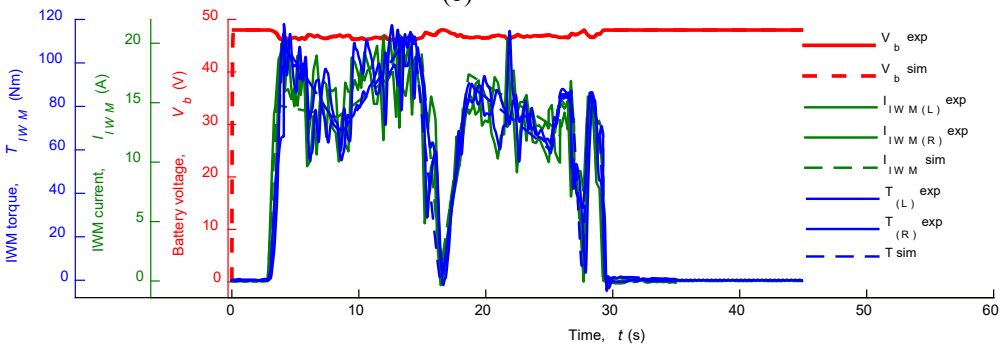

(c)

Figure 15. The evaluation of IWM-EV acceleration performance on incline road at 20 km/h: (a) throttle and braking input; (b) vehicle dynamic characteristics; (c) electrical dynamic characteristics

Appendix D

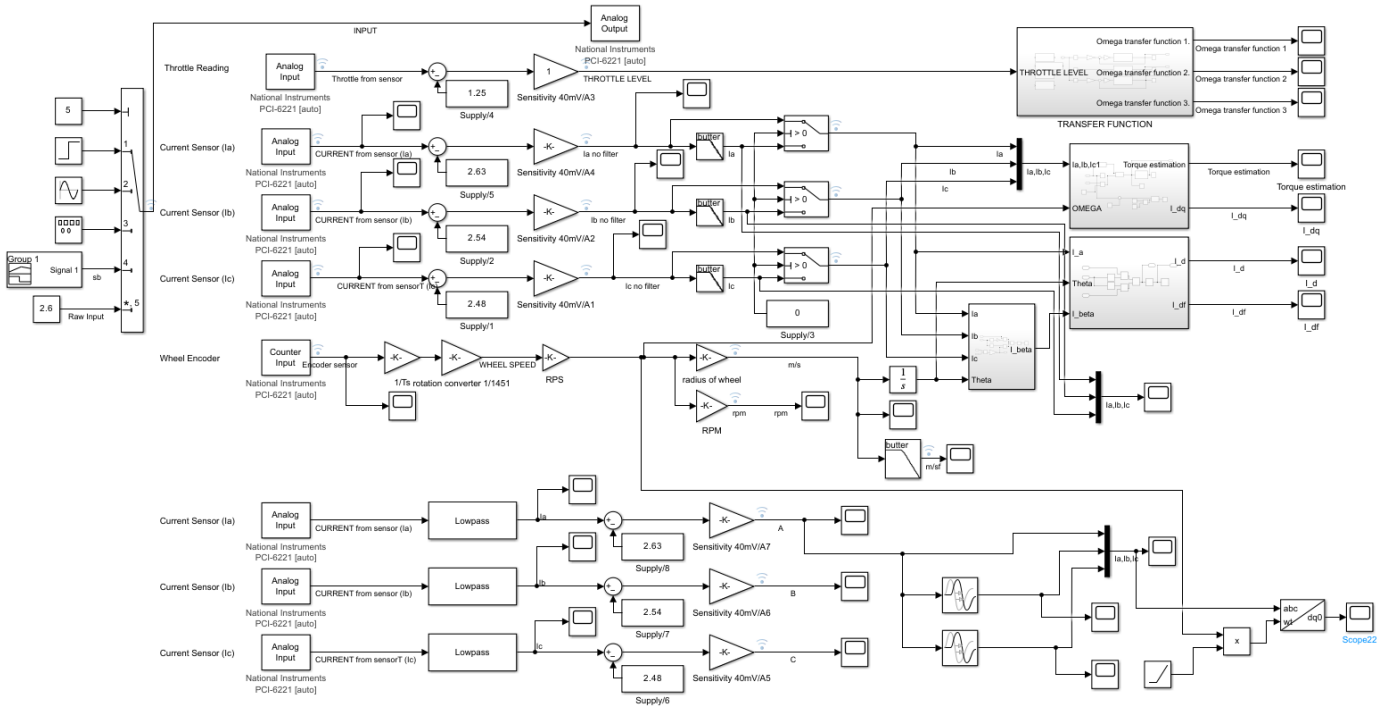

Figure 16. Experimental data logger by using MATLAB/ Simulink for IWM validation

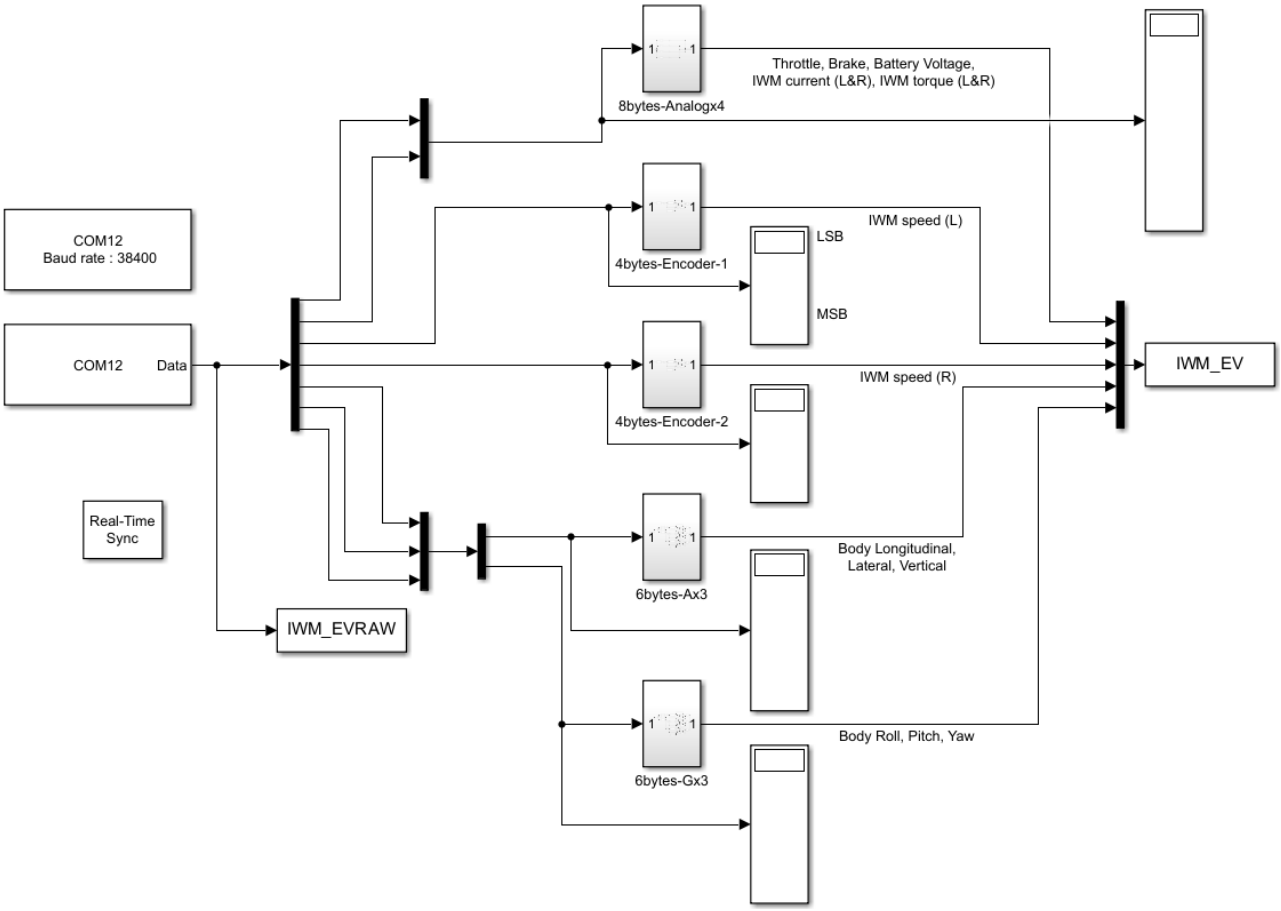

Figure 17. Experimental data logger using Arduino-MATLAB/ Simulink for IWM-EV validation

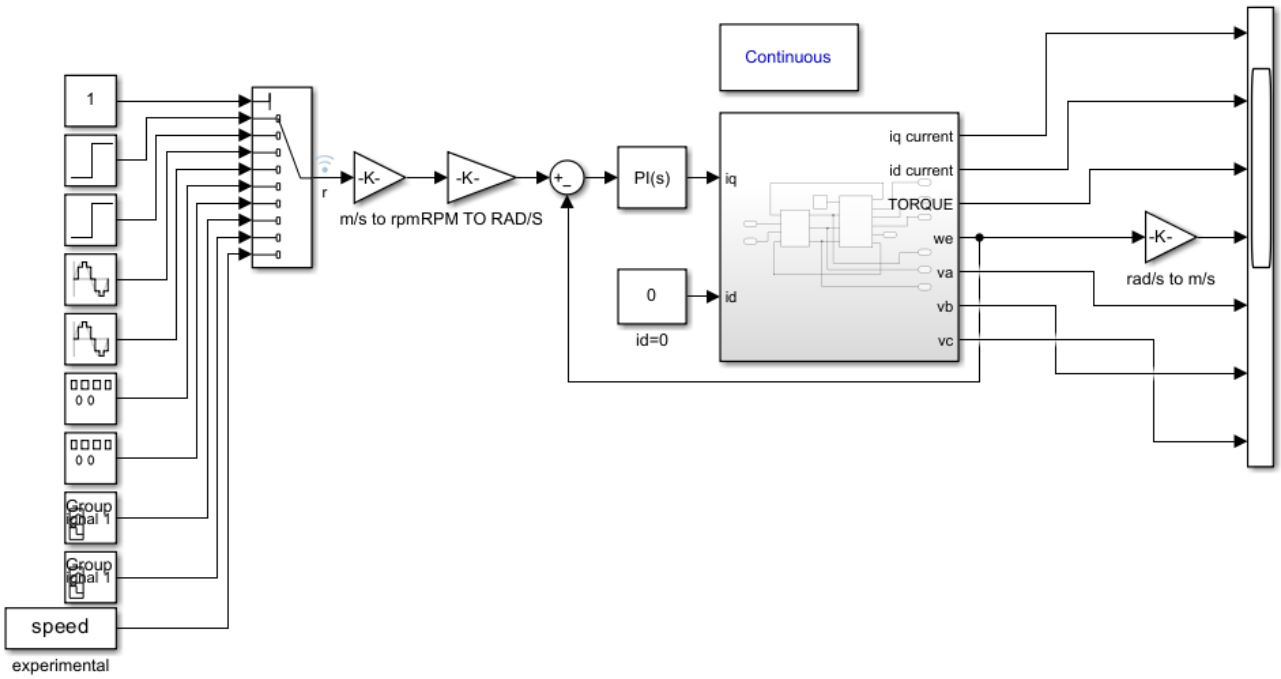

Figure 18. IWM control scheme

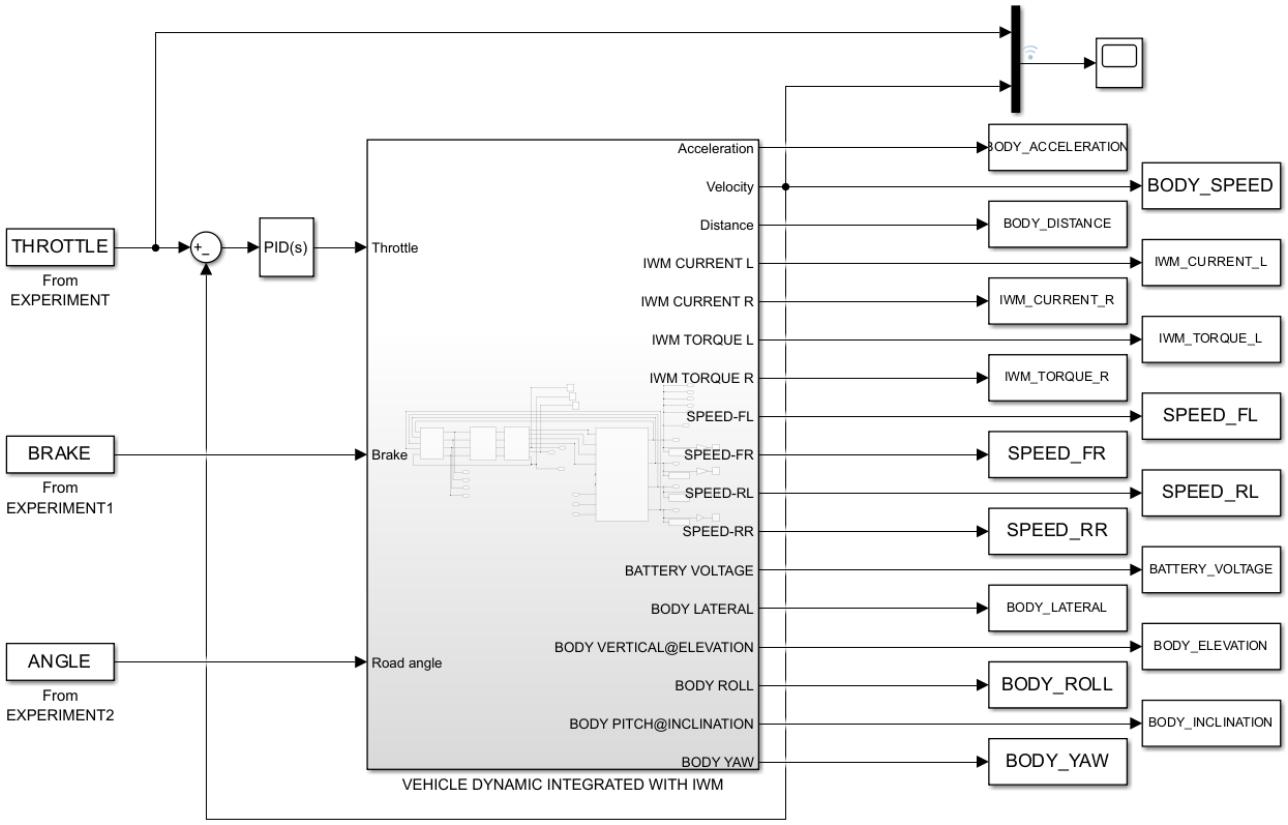

Figure 19. IWM-EV control scheme